NAVAL POSTGRADUATE SCHOOL
Monterey, California

THESIS

THE FALL TRANSITION OFF CENTRAL CALIFORNIA IN 2002

by

Colleen M. O'Malley

June 2003

Thesis Advisor:	Curtis A. Collins
Second Reader:	Mary L. Batteen

THIS PAGE INTENTIONALLY LEFT BLANK

REPORT DOCUMENTATION PAGE			Form Approved OMB No. 0704-0188
Public reporting burden for this collection of information is estimated to average 1 hour per response, including the time for reviewing instruction, searching existing data sources, gathering and maintaining the data needed, and completing and reviewing the collection of information. Send comments regarding this burden estimate or any other aspect of this collection of information, including suggestions for reducing this burden, to Washington headquarters Services, Directorate for Information Operations and Reports, 1215 Jefferson Davis Highway, Suite 1204, Arlington, VA 22202-4302, and to the Office of Management and Budget, Paperwork Reduction Project (0704-0188) Washington DC 20503.			
1. AGENCY USE ONLY *(Leave blank)*	**2. REPORT DATE** June 2003	**3. REPORT TYPE AND DATES COVERED** Master's Thesis	
4. TITLE AND SUBTITLE: The Fall Transition off Central California in 2002			**5. FUNDING NUMBERS**
6. AUTHOR(S) O'Malley, C.M			
7. PERFORMING ORGANIZATION NAME(S) AND ADDRESS(ES) Naval Postgraduate School Monterey, CA 93943-5000			**8. PERFORMING ORGANIZATION REPORT NUMBER**
9. SPONSORING /MONITORING AGENCY NAME(S) AND ADDRESS(ES) Naval Oceanographic Office Stennis Space Center, MS			**10. SPONSORING/MONITORING AGENCY REPORT NUMBER**
11. SUPPLEMENTARY NOTES The views expressed in this thesis are those of the author and do not reflect the official policy or position of the Department of Defense or the U.S. Government.			
12a. DISTRIBUTION / AVAILABILITY STATEMENT Approved for public re lease; distribution is unlimited			**12b. DISTRIBUTION CODE**

13. ABSTRACT ***(maximum 200 words)***

During the fall of 2002 the physical oceanographic conditions off Central California were monitored by means of CTD casts and VMADCP current measurements during two cruises. The first cruise, included 38 stations and one time series station. The second cruise was sponsored by the Naval Oceanographic Office (NAVOCEANOCEANO) and occupied nine sections along the coast. A total of 86 stations and two time series stations were occupied during the second cruise. CTD calibration and data processing methods are described.

The isosteres, current vectors, and salinity distribution from the cruises provide a clear picture of the circulation pattern during the fall 2002. A strong shoreward, anticyclonic meander of the California current was observed. Although the meander itself did not cross the dynamic trough that separated inshore and offshore currents, at the point where the meander was adjacent to the trough, a ridge formed which transported Subarctic waters into the coastal zone. These fresh waters were advected to the north and south along the coast, depending upon the direction of nearshore currents. The observed mesoscale circulation showed the manner in which waters which are upwelled at the coast in summer are replaced by oceanic waters in the fall and winter.

14. SUBJECT TERMS California Current System, Fall Transition, Deep Sound Channel			**15. NUMBER OF PAGES** 101
			16. PRICE CODE
17. SECURITY CLASSIFICATION OF REPORT Unclassified	**18. SECURITY CLASSIFICATION OF THIS PAGE** Unclassified	**19. SECURITY CLASSIFICATION OF ABSTRACT** Unclassified	**20. LIMITATION OF ABSTRACT** UL

NSN 7540-01-280-5500 Standard Form 298 (Rev. 2-89)
Prescribed by ANSI Std. 239-18

THIS PAGE INTENTIONALLY LEFT BLANK

Approved for public release; distribution is unlimited

THE FALL TRANSITION OFF CENTRAL CALIFORNIA IN 2002

Colleen M. O'Malley
Ensign, United States Navy Reserve
B.S., United States Naval Academy, 2002

Submitted in partial fulfillment of the
requirements for the degree of

MASTER OF SCIENCE IN PHYSICAL OCEANOGRAPHY

from the

NAVAL POSTGRADUATE SCHOOL
June 2003

Author:

Colleen M. O'Malley

Approved by:

Curtis A. Collins
Thesis Advisor

Mary L. Batteen
Second Reader

Mary L. Batteen
Chairman, Department of Oceanography

THIS PAGE INTENTIONALLY LEFT BLANK

ABSTRACT

During the fall of 2002 the physical oceanographic conditions off Central California were monitored by means of CTD casts and VMADCP current measurements during two cruises. The first cruise, between Pioneer and Hoke Seamounts, included 38 stations and one time series station. The second cruise was sponsored by the Naval Oceanographic Office (NAVOCEANO) and occupied nine sections along the coast from Pt. Reyes to just south of San Simeon. A total of 86 stations and two time series stations were occupied during the second cruise.

The isosteres, current vectors, and salinity distribution from the cruises provide a clear picture of the circulation pattern during the fall of 2002. A strong shoreward, anticyclonic meander of the California Current was observed along the offshore edge of the survey area. The meander advected Subarctic surface and intermediate waters into the region. Although the meander itself did not cross the dynamic trough that separated inshore and offshore currents, at the point where the meander was adjacent to the trough, a ridge formed which served to transport Subarctic waters into the coastal zone. These fresh waters then were advected to the north and south along the coast, depending upon the direction of nearshore currents. The observed mesoscale circulation showed the manner in which waters which are upwelled at the coast in summer are replaced by oceanic waters in the fall and winter.

Analysis of the geography of the deep sound channel (DSC) during this period showed that the mean pressure of the DSC was at 586 dbar while the mean sound speed minimum was 1480 m/s. The minimum sound speed varied 3 m/s while the pressure of the minimum varied by 330 dbars. The shape of the pycnocline controlled the pressure and depth of the DSC in the region.

THIS PAGE INTENTIONALLY LEFT BLANK

TABLE OF CONTENTS

THIS PAGE INTENTIONALLY LEFT BLANK

LIST OF FIGURES

LIST OF TABLES

THIS PAGE INTENTIONALLY LEFT BLANK

ACKNOWLEDGMENTS

Without the positive encouragement, continued advice, assistance and wealth of knowledge provided to me by my advisor, Dr. Curtis A Collins, this thesis would never have been completed. His daily mentorship taught me so many things about science, writing and perhaps most importantly about life. My admiration for him and his work grows in each interaction I have with him. I would also like to express my appreciation for Mr. Tarry Rago, who offered me continued encouragement and assistance with numerous computer programs and figures for my thesis. Additionally, I would like to thank Stewart Lamerdin, for his help on the Underway Data Acquisition (UDAS) system as well as Leonid Ivanov for his assistance with data processing. I would also like to thank some of the wonderful people in my office including Ms. Marla Stone and CDR Juan Aguilar who provided me with daily motivation and encouraging words.

The Naval Oceanographic Office sponsored the cruise from 5-19 November 2002. The support of the officers and crew of the **R/V Point Sur** is gratefully acknowledged. The Office of Naval Research sponsored the Hoke Seamount cruise from 22-31 October. We would also like to thank the Packard Foundation for supplying the data for buoy M2 which proved to be critical for this thesis.

On a personal note, I would like to thank the people in my life who have provided me with unwavering support and love. First to my parents, thank you so much. You may never know how much your love and support aided in my success. Secondly to my brothers, who provided me with comic relief and comforting phone calls. Thirdly, to my boyfriend James for his your compassion and understanding through my late nights and stressful phone calls. Finally, I would be remissed if I failed to mention my classmates in the IGEP program, to Ensigns Tjoa, Ray, Holt and Roth, thank you. It was their encouragement, which allowed me to succeed when I might have otherwise failed, and to all of them I owe a debt of gratitude.

THIS PAGE INTENTIONALLY LEFT BLANK

I. INTRODUCTION

This thesis uses two cruises from the fall of 2002 to describe ocean conditions off central California. The station pattern for these cruises is shown in Figure I-1. The first cruise, from Moss Landing to the Hoke Seamount consisted a section of 38 stations and one time series station, completed in the Gulf of the Farallones. The second cruise was sponsored by the Naval Oceanographic Office (NAVOCEANO) and was based upon the California Cooperative Fisheries Investigations (CalCOFI) protocol. A total of 86 stations and two time series stations were occupied during the second cruise. Although it was necessary to calibrate data collected on the cruises, most efforts went into interpretation of the hydrographic data. Results show an onshore meander or eddy of the California Current spreading warm fresh waters inshore. These results are placed in the context of regional ocean processes below.

A. CALIFORNIA CURRENT SYSTEM

The California Current System (CCS) is comprised of two flow regimes. One is a broad, shallow, equatorward current, called the California Current (CC). This current extends for approximately 1000 km from shore (Hickey 1998). Located to the east of the North Pacific gyre, the CC) transports 10-20 Sverdrups of water at ~25 cm/s equatorward. The maximum current velocities are found at or near the surface (Lynn and Simpson 1987). As a surface current, its properties generally extend from the surface to approximately 300 m in depth. The second flow regime, within 150 km of the coast, consists of two narrower poleward boundary currents, the Inshore Current (IC) and the California Undercurrent (CU) (Lynn and Simpson, 1987; Collins et al., 1997). The California Undercurrent originates near the southern tip of Baja California and is poleward along the coast. Varying with season, strength, core depth and position, the CU is a fairly narrow, high-speed flow (Lynn and Simpson, 1987). The IC forms seasonally in the fall and winter (Lynn and Simpson 1987). North of Point Conception the IC is labeled the Davidson Current. The water the currents carry characterizes the flows (Lynn and Simpson 1987).

The CCS is primarily composed of four water masses, the Pacific Subarctic water carried southward by the California Current, Eastern North Pacific Central water, Equatorial Pacific water, and the North Pacific Intermediate water (Lynn and Simpson 1987). The water masses of particular interest for this study are the Pacific Subarctic water, the North Pacific Intermediate water and the Equatorial Pacific water (subsurface water masses). Forming at areas of high latitudes where a high level of precipitation falls and heat loss is great, the Pacific Subarctic water enters the California Current around 48^{o} N (Pickard and Emery, 1964). With a recognizably low salinity, high phosphate, and high dissolved oxygen, the Pacific Subarctic water is distinguishable throughout the CCS. The Equatorial Pacific water enters the California Undercurrent from the south, originating in the tropical Pacific. Possessing high salinity, high nutrients and low dissolved oxygen, the Equatorial Pacific water dominates an entirely different region of the water column and consequently a different region of the temperature-salinity diagram. Next to the coast, a fifth water mass is formed during spring and summer as upwelled waters warm at the sea surface. The properties of North Pacific Intermediate water mix with those of the Equatorial waters described above. Coastal waters are thus transition zones between the fresher surface and intermediate Subarctic waters and the saltier coastal up-welled surface and intermediate equatorial waters.

The coastal zone is high in eddy kinetic energy (EKE) (Miller et al. 1990). A maximum EKE occurs near the coast in early summer and moves offshore in late summer and fall (Miller et al. 1999). Surface current and sea surface temperature (SST) data show jets, squirts and eddies forming over the region. Typically these features are associated with topographic features such as headlands and are responsible for transporting materials away from the coast. EKE decreases offshore, which could be due to energy dissipation in the deep ocean, producing a diminished surface signature (Miller et al. 1999).

B. SPRING TRANSITION

Between winter and spring a dramatic and abrupt transition occurs within the CCS. The change in water properties is labeled the spring transition (Hickey 1998). Driven by changes in the wind-field, the transition causes the isopycnals to slope up

towards the coast, with a subsequent drop in sea level (~10 cm) and a reversal in the nearshore currents (Fig I-2). The transition occurs over a large scale, covering approximately 800 km (Hickey 1998). The response is generally stronger in the northern latitudes. Off the coast of northern California, the changes seem to be driven by strong equatorward winds; however to the south, off the Southern California Bight, the winds tend to be significantly weaker (Hickey 1998). The change in wind conditions forces both a local response and a remotely forced response (Hickey 1998). The minimum sea level moves poleward along the coast. As the waters pile up to the north it creates a downslope in the sea level, which in turn forces an equatorward flow offshore (Hickey 1998).

C. FALL TRANSITION

Less dramatic than the spring transition, the change between summer and winter occurs over an extended time period and is labeled the fall transition (Johnson 1990). Locally, sea level decreases about 4 cm from 1 September (day 242) to 15 November (day 319) (Fig I-2). Sporadic and gradual halting of coastal upwelling causes a gradual increase in SST and signals the beginning of the transition. Accompanied by the deepening of the Aleutian Low, fall transitions usually occupy the upper 200 m of the water column (Johnson 1990). While some changes may occur abruptly, such as changes in sea level, others change over a period of months (coastal upwelling indicators and SST) (Johnson 1990). Since the fall transition is less dramatic than spring, it is usually considered part of a gradual annual cycle and has been the focus of only a few studies.

D. ORGANIZATION OF THESIS

The goal of this thesis is to describe the fall transition off the central California coast in 2002. Background information for the CCS and the spring and fall transitions are discussed above. Chapter II discusses the cruise design, conductivity, temperature and depth (CTD) data, vessel mounted acoustic Doppler current profiler (VMADCP), underway data acquisition system (UDAS), the temporal variability, and principal component analysis. Results are shown for the water properties, the upper and lower salinity minimums, isopycnal and isobaric surfaces, and the ADCP data in Chapter III.

Chapter IV summarizes results and presents conclusions. Appendix D discusses the deep sound channel.

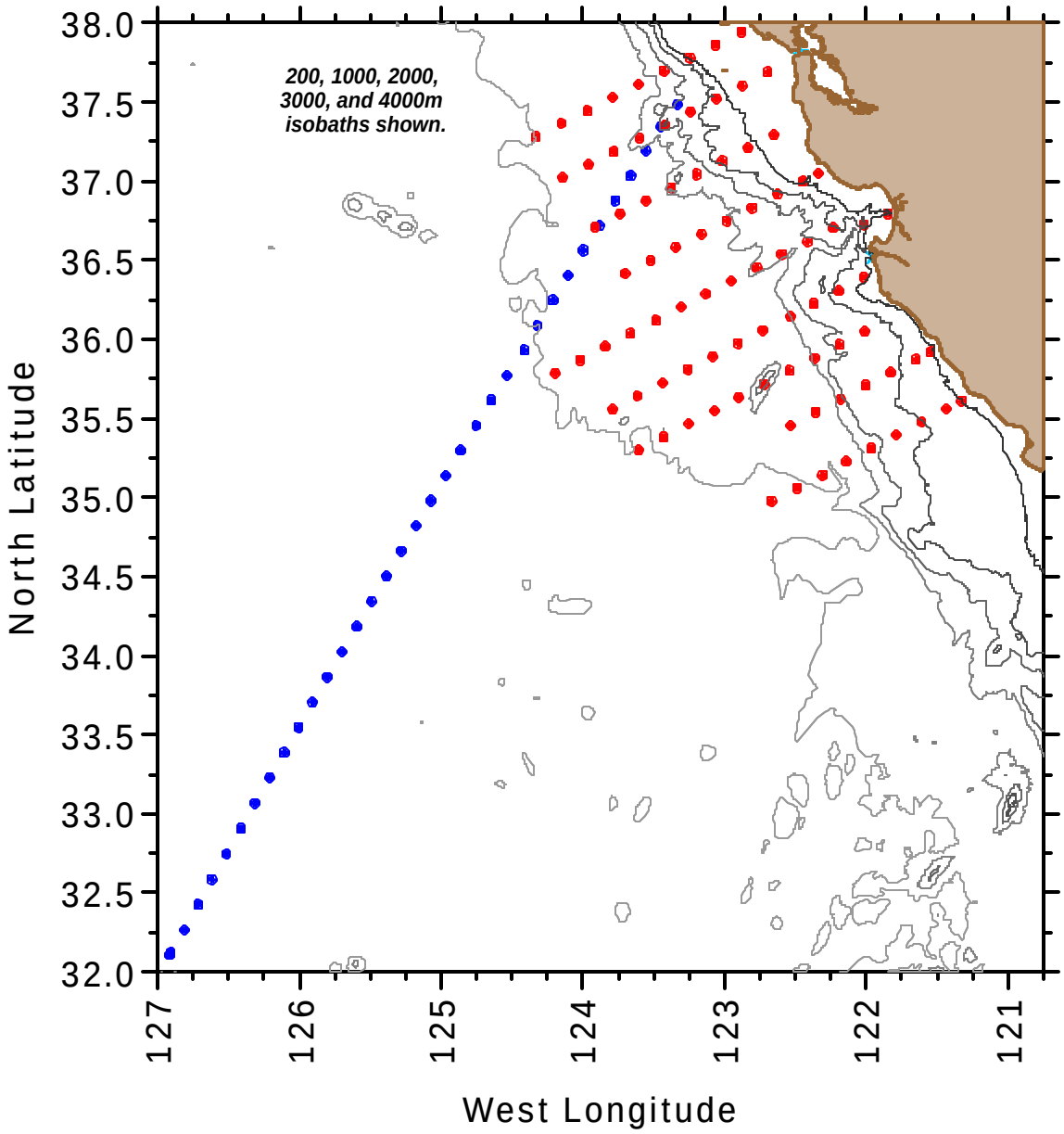

Figure I-1. CTD stations for the NAVOCEANO Cencal (red) and Hoke Seamount (blue) cruises.

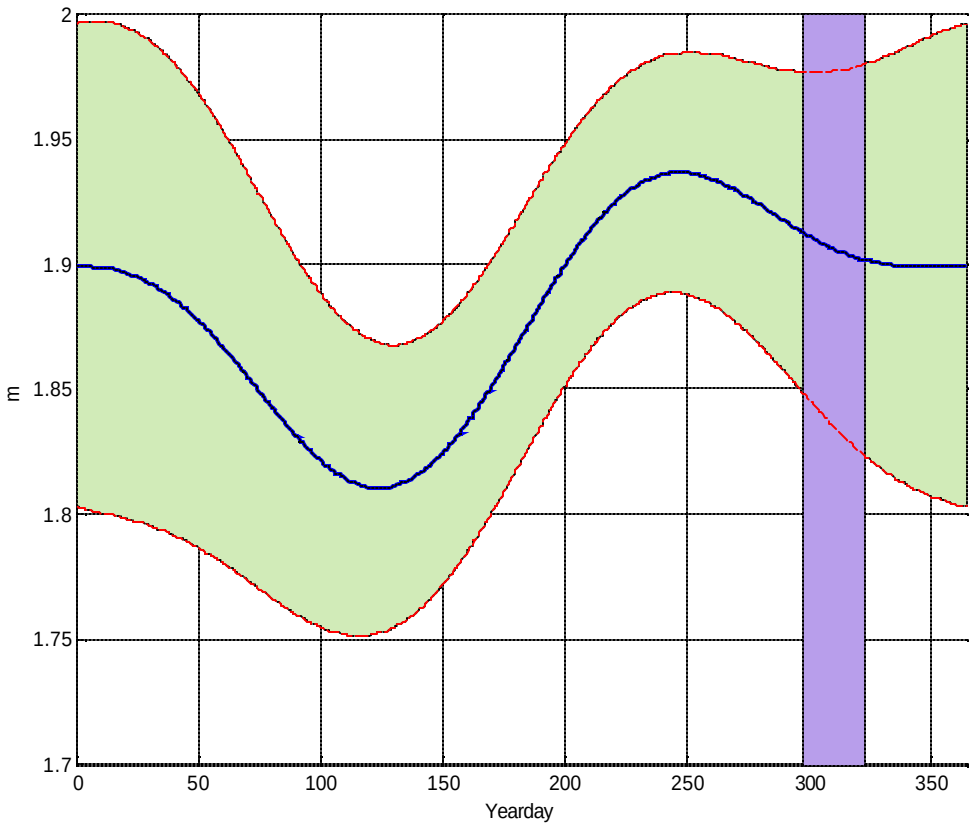

Figure I-2. Annual cycle of daily mean sea level from 1974-2001 (referenced to mean lower low water) for Monterey, CA. Green shaded area represents plus/minus one standard deviation and the purple shaded area represents the time period of cruises discussed in this thesis (22 Oct-19 Nov 2002).

II. DATA AND METHODS

CTD data collected during two research cruises in the fall of 2002 are the principal basis for this thesis. Data from the VMADCP, satellite imagery, and M2 will also be used. M2 is a buoy outside of Monterey Bay, maintained by Monterey Bay Aquarium Research Institute (MBARI).

A. CRUISE DESIGN

The data for this thesis was collected during two oceanographic surveys off Central California in the fall of 2002. The first cruise, from Moss landing to the Hoke Seamount, took place from 22-31 October 2002. During this cruise, a section of 38 CTD stations were occupied and one time series station was completed in the Gulf of the Farallones. The CTD stations, at about 20 km spacing, ran along the geodesic in a direction of about 305^{o} from the Hoke Seamount to the NOAA acoustic array on Pioneer Seamount and thence to the continental shelf (Fig I-1). The second cruise was sponsored by the Naval Oceanographic Office (NAVOCEANO), and took place from 5-19 November 2002. The station pattern for the NAVOCEANO cruise was based upon the California Cooperative Fisheries Investigations (CalCOFI) protocol. (The CalCOFI protocols were adopted for numerous scientific surveys, beginning in 1950). CTD's were cast in approximately equidistant lines, at approximately 40 km spacing, running perpendicular to the coastline. This survey occupied nine of these lines with varying numbers of CTD stations per line and a total number of 86 CTD stations. Two 25-hour "anchor" stations were also completed on the NAVOCEANO cruise. The spatial survey was interrupted by a severe storm from days 311 to 313 and the first time series was collected in San Fransisco Bay during this storm. The second time series was collected in Carmel Bay at the end of the spatial survey. The station coordinates, cast depth, cast time, and station numbers for both cruises are given in Tables 1 and 2.

B. CTD DATA

The SeaBird 911*plus* CTD was used to measure the conductivity, temperature and pressure at each hydrographic station. Measurement accuracy was 0.001°C , 0.3 dbars and 0.0003 S/m. During the cruise, water samples were collected on each CTD cast and subsequently processed with a laboratory salinometer to assure accurate conductivity measurements. Where depth permitted, data was collected to 1000 m (6 deep water stations extended to near the bottom on the Hoke cruise).

The CTD data was processed using SeaBird software into a table of 2 dbar bins for each cast (JPOTS editorial panel, 1991). SeaBird and MATLAB™ software subsequently derived seawater quantities from these 2 dbar tables including specific volume anomaly, density anomaly, and geopotential anomaly using the 1980 Equation of State (Fofonoff, 1985).

Temperature calibration information, obtained from a SeaBird post-cruise calibration report, was compared to the pre-cruise calibration for both the primary and secondary temperature sensors. The primary temperature sensor 2673 was calibrated prior to the cruise on 02 April 2002 and following the cruise on 12 December 2002. The equation used to calculate the ITS-90 temperatures, where g, h, i, j and f_o are determined by calibration was:

$$Temp(ITS-90) = [\{g + h[\ln \frac{f_0}{f}] + i[\ln^2 \frac{f_o}{f}] + j[\ln^3 \frac{f_o}{f}]\} - 273.15]^{-1}$$

The drift since the last calibration was +0.00420 °C/year. The temperature plotted against temperature difference was about 3 m°C, at 20°C (Fig II-1). The secondary temperature sensor (2632) had significantly less drift. It was calibrated prior to the cruise on 04 January 2001 and following the cruise on the same day as the primary sensor. The drift on the secondary sensor since the last calibration was -0.00007 °C/year. The pre and post temperature difference is plotted in Figure II-1 (lower). The secondary sensor had only 5% of the difference reported for the primary sensor, about 0.13 m°C at 20°C.

A similar comparison was completed to evaluate pressure. The pressure sensor was calibrated pre-cruise on 09 December 1997 and calibrated again post-cruise on 17

December 2002. The pressure calibration reports, completed by SeaBird, provided slope and offset values for use in the SEASOFT programs. For a range of 0-1000 dbars, the values for the pre and post cruise calibration numbers were plotted against the pressure difference in dbars. The results showed only a small pressure difference, approximately 0.2 dbars, at 1000 dbars.

The next calibration was that of the primary and secondary conductivity sensors. The primary conductivity sensor (395) was calibrated prior to the cruise on 17 Jan 2002 and then following the cruise on 12 December 2002. The secondary sensor (434) was calibrated on the 25 January 2002 and again on the same day as the primary conductivity sensor. The post cruise conductivity was plotted against the difference in conductivity between the two calibrations in MATLAB™ for both the primary and secondary sensors. The results from the primary sensor showed a difference of about 2 mS/m and a difference of about 3 mS/m for the secondary sensor (Fig II-2). Since the last calibration, the primary sensor had drifted -0.00060 S/m/month. The secondary sensor had a slightly larger drift between calibrations of -0.00100 S/m/month.

The final step in the CTD calibration involved a comparison between conductivities from water samples collected during the CTD cast to those recorded by the CTD. The CTD values were determined for both the pre and post temperature calibrations of the primary (T0) and secondary (T1) temperature modules and the primary (C0) and secondary (C1) conductivity cells. Post cruise results were much better than the pre cruise calibrations. The post cruise calibration was then used to produce four sets of linear regressions for the true conductivity (C) as follows:

Hoke:

C(T0) vs C0: Slope = 0.0000360776, Offset = -0.0002540595

C(T0) vs C0: Slope = 0.0004385912, Offset = -0.0013553385

C(T0) vs C1: Slope = 0.0000868949, Offset = -0.0000008185

C(T1) vs C1: Slope = 0.0004892783, Offset = -0.0011001271

NAVOCEANO:

C(T0) vs C0: Slope = 0.0000659829, Offset = -0.0004587278

C(T0) vs C0: Slope = 0.0000659829, Offset = -0.0004587278

C(T0) vs C1: Slope = 0.0001745380, Offset = -0.0001307862

C(T1) vs C1: Slope = 0.0006265789, Offset = -0.0014685762

Inspection shows that the best results were obtained for the primary temperature and conductivity sensors.

Comparisons between bottle results and the primary conductivity sensor are shown in Figure II-3. The upper two graphs show the conductivity difference plotted by date (Fig II-3, upper left) and alphabetically by case (Fig II-3, upper right). It is clear that the conductivity difference did not vary during sampling analysis, eliminating any possibility of analysis data bias. Values exceeding two standard deviations (σ) were removed from the lower graphs. Figure II-3, lower left shows little variation in primary true conductivity over values of true conductivity. The black line is the linear fit of the data based on the slope and offset calculated (the C(T0) vs C0 equation given above for NAVOCEANO). A slightly positive slope existed. Clearly the deep-water stations had a lower true conductivity, of about 3.3 S/m, while the true conductivity for the shallow-water stations extended over a range of true conductivities from about 3.3-4.3 S/m. Figure II-3, lower right shows primary true conductivity by CTD station number and demonstrates the distribution of deep and shallow water stations in terms of conductivity difference. The Hoke and NAVOCEANO cruises show similar results.

To summarize, the pre-cruise SeaBird sensor calibrations showed significant error when the pre and post cruise calibrations were being compared. The large temperature change in the primary temperature (T0) sensor flagged a possible problem with the data. As a result, the data was re-processed using post-cruise calibrations. Analysis of post

cruise calibrated data showed the best results for conductivity were obtained using the primary temperature (T0) and primary conductivity (C0). The standard deviation for the salinity difference was +0.0026 for NAVOCEANO and +0.0019 for Hoke, both within system error (0.003). Since conductivity is also a function of temperature, this provided confidence that the post-cruise calibration for the primary temperature sensor (T0) was reasonable.

C. VMADCP

Upper ocean currents were measured with a VMADCP. The VMADCP is a RDI 150 kHz narrow band instrument. Data were collected using the RDI data acquisition system. Shipboard navigation information was integrated into the data system using the University of Hawaii user-exit-4 program. Currents were resolved into 8 m bins from 15 m to ~400 m when water depth permitted. Currents were sampled at one-second intervals and averaged over five-minutes. During the cruises, special attention was paid to the VMADCP to make sure that bottom tracking was used when the bottom appeared on the VMADCP monitor or when water was shallower than 400 m. Navigation information included GPS corrections for gyrocompass variations (Pollard and Read, 1989) that were measured with an Ashtech system with a resolution of 0.1 degrees.

Raw VMADCP data were loaded into a CODAS database and processed using software developed at the University of Hawaii. The VMADCP temperature measurements did not work properly. Sea surface temperature and salinity measurements using a higher resolution (0.01C, S=0.01) SeaBird sensors were used. These are located on a seawater loop that draws water through a sea chest that was located next to the VMADCP. VMADCP calibration programs yielded 158 (385) samples for water track (bottom track) with an amplitude correction of 1.0115 ± 0.0075 (1.0148 ± 0.0051) and a phase correction of 1.8605 ± 0.4965 (1.8456 ± 0.2493) (Joyce, 1989) which were subsequently applied. Finally, the data were averaged over one-hour periods and 50 m vertical bins. Results are accurate to 1-2 cm/s (Chereskin and Trunnell, 1996).

D. UDAS

Meteorological and sea surface data were collected continuously with an underway data acquisition system (UDAS). The UDAS consists of a series of modules that are polled sequentially. In the order they were sampled, these modules were:

Furuno GPS, Ashtech GPS, R.M Young meteorological suite, SeaBird Electronics thermosalinograph, and NPS supplied boomprobe. The modules, which were used for this thesis, are the Ashtech GPS, the R.M Young meteorological suite, and the SeaBird Electronics thermosalinograph.

The GPS modules record and display the ship's position and related parameters. This data is not manipulated in any way and is simply displayed and recorded as the satellite receiver provided it. Furuno and Ashtech manufacture the two GPS systems used in the UDAS and both signals are differentially corrected (Lamerdin, personal communication).

The R.M. Young meteorological module displays and records the ship's meteorological data. Each of the sensors in this suite is sampled twice with a two second delay between samples. The sampling rate is limited by the speed at which the data is output by the R.M. Young programmable translator. The course and speed over ground, used in the averaging of wind directions, is taken from the Furuno GPS. The ship's heading is taken from the ship's gyrocompass and is averaged along with the rest of the meteorological data. The meteorological sensors are not routinely calibrated. Twice each year, NPS places an independent meteorological system on the ship. Comparison of the data collected by the NPS meteorological sensors and the ship's sensors is made to validate UDAS measurements (Lamerdin, personal communication).

The SeaBird Electronics thermosalinograph module consists of measurements of temperature, conductivity, salinity and fluorescence. The temperature is sampled from water collected at the hull, amidships, before it is pumped up to the main lab. Due to the draft of the ship, this water is collected at roughly 3 m below the surface. Conductivity, salinity and fluorescence are sampled in the main lab. Three measurements are taken from each of these sensors. This averaged number is then displayed and recorded. Samples are taken every six seconds due to the output rate on the thermosalinograph.

There is no set schedule for the calibration of the temperature and conductivity sensors in this system. The ship sends these sensors back to SeaBird for calibration roughly twice a year, however, sensors are replaced when measurements appear to be questionable when compared to the ship's CTD sensors. A comparison of the temperature and salinity between the ship's CTD and UDAS is recorded at the start of every CTD cast. The ship's fluorometer outputs a raw voltage for fluorescence units. If a researcher is interested in converting voltage measurements to actual fluorescence concentration measurements, it is their responsibility to calibrate this instrument (Lamerdin, personal communication).

Measurements are recorded when each module is finished collecting and processing the data. Approximately 30 seconds is required to run through one cycle. Files are broken into 24-hour periods and are given filenames indicating the GMT date during which the data was collected (Lamerdin, personal communication). SST and salinity for both cruises, are discussed in detail in Appendix A.

The wind data, which was recorded by the R.M. Young meteorological suite, is displayed in Figure II-4 for each cruise. During the Hoke Seamount cruise the winds blew steadily from the northwest, but the observed winds on the northern portion of the track were significantly stronger than those on the southern and eastern legs. The winds during the NAVOCEANO Cencal cruise changed magnitude and direction at or just north of Monterey Bay (along CALCOFI Line 67). South of Monterey Bay the winds blew steadily from the northwest and increased in magnitude with decreasing latitude. North of Monterey Bay the winds were from the southeast, but sometimes varied in direction. The winds at and just north of Monterey Bay were weaker and highly variable. Temporal variability was likely the cause of many of the changes in Figure II-4 and will be discussed next.

E. TEMPORAL VARIABILITY

The cruises were separated by five days between the end of the Hoke cruise and the beginning of the NAVOCEANO Cencal cruise. To determine whether the data was collected on a time scale which allowed it to be considered as one data set rather than two separate data sets, the two stations occupied on both the Hoke and the NAVOCEANO cruises are examined. Figure II-5 shows the temperature-salinity diagrams for the two

stations. The first station was located on Line 61.5 of the NAVOCEANO cruise at approximately 37^o 21 N, 123^o 26 W. The second station was located on Line 63 at approximately 36^o 43 N, 123^o 54 W.

In comparing the two data sets, separated by five days, apparent differences can clearly be seen. From the surface to the thermocline, it is apparent at both locations that the time lag caused some fairly large changes in salinity at and above the thermocline. The time lag between cruises is approximately 12 days. At station 61.5-60, differences show the freshening associated with the fall transition, with a lowering of salinity. Station 63-70 shows an increase in salinity, perhaps associated with the passage of the storm on days 311-313.

The change in water properties between cruises suggests that it may not be possible to combine the cruise data into a single synoptic data set. To further address the synopticity, the data collected at M2 was used. M2 is a buoy located outside the mouth of the Monterey Bay (Fig II-6, upper) along CALCOFI Line 67 (MBARI 2002). In Figure II-6 (lower) the movement of buoy M2 around its watch circle is shown during the period of the cruises. The green lines indicate movement prior to year day 305.5 and the red lines indicate the buoy's movement from year day 305.5 until year day 340. M2 was located along the southern arc of its watch circle in October. The movement of M2 was more variable during the month of November, an indication that the circulation pattern changed. M2's northward movement due either to poleward surface current or northward wind, although restricted by mooring, was suggestive of the circulation pattern associated with the fall transition.

Figure II-7 is the same figure as Fig I-2, with the sea level for October-November 2002 overlaid. The sea level dropped over the time period of the cruises with the exception of a single spike, which corresponded to the passage of the storm on days 311-313. The gradual decrease in sea level, cessation of coastal upwelling and southward wind, results in a nearshore circulation pattern with the flow moving poleward at the surface along the coast.

The halting of coastal upwelling resulted in a gradual and continuous rise in the water temperature, shown in Figure II-8 (top). The middle panel shows the salinity

stratification with depth. There was a disturbance followed by a deepening in the halocline and shoaling of the thermocline on and after yearday 305. Following the change in stratification there were several oscillations in the halocline. The density anomaly versus spice (Fig II-8, bottom) showed cores of low spice water after yearday 305, which corresponded to the changes in the temperature and salinity described above. The spice change indicated the presence of a different water mass.

Observation of M2's current measurements and winds reveal a stark contrast between the months of October and November. M2 current profiles are shown in Figure II-9. There was an apparent shift in current direction around year day 305, which marks the start of November 2002. This shift is most easily seen in the north-south component of the current profile. The velocities shift from southward to northward, defining a clear difference in nearshore circulation between the months of October and November, and consequently the two cruises. Prior to day 310 the winds at M2 (Fig II-10) consistently blew to the southeast. At days 311-313, there was a strong reversal in the winds due to the passage of the storm described earlier. Following the storm, the winds are less consistent and switch between blowing to the southeast and the southwest.

The differences between October and November were consistent between shipboard winds, coincident CTD stations and coastal observations at M2. A cessation of coastal upwelling, changes in wind direction and sea level were consistent with the pattern of the fall transition. The variability between the two data sets, caused by the synoptic lag, was significant. Therefore, the two data sets will be examined separately in Chapter III.

F. PRINCIPAL COMPONENT ANALYSIS (PCA)

Principal component analysis (PCA) is a method of describing or evaluating a data set. PCA decomposes a variable into its modes or principal components which, when combined, account for 100% of the variability. The first three principal components plots usually account for about 80-90% of the total variability or variance (the method is described by Jackson, 1991). In oceanography PCA is sometimes called empirical orthogonal function (EOF) analysis. The term EOF was first attributed to Lorenz by Emery and Thompson (1997) in the development of the technique for

statistical weather prediction. Two advantages of EOF analysis are that "...EOF's provide the most efficient method of compressing the data and they may be regarded as orthogonal modes of variability of the data field (Emery and Thompson, 1997)." The first few EOF's can be used to reconstruct the data field, eliminating unwanted variability (that which is not coherent over the data grid). EOF analysis is similar to Fourier analysis and EOF's are considered Fourier trigonometric functions for a homogenous time series, which is sampled at even increments. In this thesis, EOF's will be used to describe the horizontal variability of salinity and sound velocity profiles.

Table 1. Hoke CTD Stations

Latitude (N)	Longitude	CTD Depth	Station #	Time (UTC)
32-07.35	126-54.46	1012.0	CTD 1	1150-1238
32-06.49	126-54.44	765.0	CTD 2	2121-2205
32-15.94	126-48.66	1011.8	CTD 3	0227-0310
32-25.59	126-42.92	1010.0	CTD 4	0518-0557
32-35.16	126-37.11	1010.0	CTD 5	0742-0834
32-44.80	126-30.94	1012.0	CTD 6	1021-1109
32-54.38	126-24.76	1010.0	CTD 7	1336-1420
33-04.06	126-18.68	1012.0	CTD 8	1605-1643
33-13.73	126-12.53	1012.0	CTD 9	1822-1859
33-23.16	126-06.52	1012.0	CTD 10	2054-2134
33-32.77	126-00.34	4328.0	CTD 11	2320-0237
33-42.34	125-54.37	1014.0	CTD 12	0426-0506
33-51.93	125-48.18	1012.0	CTD 13	0651-0729
34-01.49	125-41.96	1012.0	CTD 14	0914-1001
34-11.00	125-35.65	4594.0	CTD 15	1149-1457
34-20.63	125-29.58	1010.8	CTD 16	1703-1740
34-30.11	125-23.25	1012.0	CTD 17	1928-2007
34-39.73	125-17.00	1012.0	CTD 18	2202-2245
34-49.26	125-10.61	4444.0	CTD 19	0030-0320
34-58.78	125-04.47	1016.0	CTD 20	0456-0535
35-08.27	124-58.04	1012.0	CTD 21	0711-0750
35-17.78	124-51.65	1012.0	CTD 22	0935-1021
35-27.28	124-45.14	4276.0	CTD 23	1203-1447
35-36.79	124-38.77	1010.0	CTD 24	1637-1712
35-46.33	124-32.24	1010.0	CTD 25	1858-1940
35-55.85	124.24.77	1014.0	CTD 26	2109-2148
36-05.28	124-19.25	3890.0	CTD 27	2332-0203
36-14.81	124-12.73	1012.0	CTD 28	0327-0406
36-24.26	124-.0624	1010.0	CTD 29	0533-0611
36-33.75	123-59.73	1012.0	CTD 30	0744-0824
36-43.15	123-53.04	3782.0	CTD 31	1020-1301
36-52.66	123-46.27	1012.0	CTD 32	1454-1534
37-02.12	123-39.77	1014.0	CTD 33	1720-1800
37-11.62	123-33.41	1010.0	CTD 34	1947-2026
37-20.66	123-26.85	1012.0	CTD 35	2208-2249
37-29.21	123-20.04	1012.0	CTD 36	0152-0233
37-37.73	123-14.19	1012.0	CTD 37	0500-0536
37-43.46	123-10.10	364.0	CTD 38	0648-0704
37-38.00	123-00.68	104.0	CTD 39	0818-0825
37-37.93	123-00.47	106.0	CTD 64	0917-0926

Table 2. NAVOCEANO CTD Stations

Latitude	Longitude	Dist Shore	CTD (dbars)	Station	CALCOFI Line #	Time
37-41.35	122-41.77	19.7810	32.0	CTD 1	61.5	0055-0100
37-56.74	122-52.89	7.6375	42.0	CTD 2	60	0255-0304
37-51.75	123-03.87	26.1560	84.0	CTD 3	60	0410-0420
37-46.77	123-14.67	44.3415	130.1	CTD 4	60	0528-0539
37-41.80	123-25.60	62.9068	1012.0	CTD 5	60	0647-0730
37-36.71	123-36.40	81.2210	1010.2	CTD 6	60	0839-0919
37-31.73	123-47.30	99.7025	1012.0	CTD 7	60	1033-1111
37-26.78	123-58.08	118.0278	1012.0	CTD 8	60	1223-1302
37-21.87	124-09.08	136.5739	1012.0	CTD 9	60	1412-1452
37-16.78	124-19.88	155.0511	1010.0	CTD 10	60	1606-1645
37-01.34	124-08.52	38.0588	1012.0	CTD 11	61.5	1849-1931
37-06.27	123-57.64	56.4215	1010.0	CTD 12	61.5	2038-2122
37-11.28	123-46.90	74.8229	1012.0	CTD 13	61.5	2218-2258
37-16.23	123-35.97	93.4337	1012.0	CTD 14	61.5	0005-0043
37-21.23	123-25.20	111.7975	1010.0	CTD 15	61.5	0148-0233
37-26.33	123-14.34	130.3283	1012.0	CTD 16	61.5	0339-0421
37-31.29	123-03.53	148.6806	536.0	CTD 17	61.5	0526-0555
37-36.25	122-52.28	167.1725	76.0	CTD 18	61.5	0701-0709
37-49.05	122-28.43	Time S	86.0	CTD 19	GGTSs	1529-1533
37-49.01	122-28.53	Time S	96.0	CTD 47	GGTSe	1657-1702
37-17.52	122-39.09	25.1993	92.6	CTD 48	63	1928-1935
37-12.68	122-50.09	43.7793	280.0	CTD 49	63	2057-2111
37-07.63	123-00.88	62.2800	682.0	CTD 50	63	2229-2254
37-02.59	123-11.74	80.8242	1014.0	CTD 51	63	0004-0043
36-57.61	123-22.58	99.3727	1012.0	CTD 52	63	0152-0229
36-52.61	123-33.31	117.8218	1012.0	CTD 53	63	0336-0419
36-47.62	123-44.11	136.2483	1012.0	CTD 54	63	0525-0609
36-42.60	123-54.80	154.6596	1012.0	CTD 55	63	0718-0759
36-24.88	123-42.14	3.6053	1014.0	CTD 56	65	1021-1058
36-29.95	123-31.29	12.4699	1012.0	CTD 57	65	1207-1244
36-34.97	123-20.52	30.6628	1012.0	CTD 58	65	1353-1432
36-39.93	123-09.85	48.9056	1010.0	CTD 59	65	1543-1619
36-44.94	122-59.03	67.2894	1012.0	CTD 60	65	1731-1812
36-49.87	122-48.27	85.8143	1012.0	CTD 61	65	1925-2005
36-54.99	122-37.67	104.1003	1012.0	CTD 62	65	2123-2203
36-59.97	122-26.86	122.6163	124.0	CTD 63	65	2321-2329
37-02.93	122-20.26	141.3079	62.0	CTD 64	65	0017-0022
36-47.64	121-50.77	9.5588	252.4	CTD 65	67	0447-0505
36-43.54	122-00.91	23.7463	1012.0	CTD 66	67	0613-0659
36-42.27	122-14.01	40.8378	1012.0	CTD 67	67	0815-0857
36-37.16	122-24.75	59.3464	1012.0	CTD 68	67	1018-1100
36-32.27	122-35.70	78.0549	1010.2	CTD 69	67	1221-1302
36-27.19	122-46.41	96.6447	1012.0	CTD 70	67	1412-1456
36-22.20	122-57.12	115.1118	1012.0	CTD 71	67	1601-1648
36-17.20	123-07.93	133.6486	1010.0	CTD 72	67	1807-1853
36-12.24	123-18.47	151.8467	1012.0	CTD 73	67	2003-2045
36-07.21	123-29.04	170.2079	1010.0	CTD 74	67	2155-2237
36-02.19	123-39.82	188.8092	1012.0	CTD 75	67	2351-0031
35-57.18	123-50.54	207.3639	1010.0	CTD 76	67	0146-0229
35-52.20	124-01.06	225.6968	1012.0	CTD 77	67	0339-0423

35-47.21	124-11.66	244.0804	1010.1	CTD 78	67	0534-0619
34-58.56	122-40.15	10.4257	1010.0	CTD 79	73	0925-1002
35-03.66	122-29.32	21.2516	1010.9	CTD 80	73	1236-1317
35-08.37	122-18.50	39.5610	1010.5	CTD 81	73	1450-1533
35-13.58	122-08.34	57.9794	1012.1	CTD 82	73	1707-1751
35-18.69	121-57.85	76.5214	1010.0	CTD 83	73	1919-1958
35-23.68	121-47.20	94.9197	1020.0	CTD 84	73	2116-2154
35-28.65	121-36.60	113.0891	986.0	CTD 85	73	2311-2345
35-33.68	121-26.06	131.6616	600.5	CTD 86	73	0100-0122
35-36.62	121-19.63	150.5650	204.0	CTD 87	73	0213-0223
35-55.27	121-32.66	7.1275	390.0	CTD 88	71.5	0506-0521
35-52.31	121-38.95	16.4754	734.0	CTD 89	71.5	0612-0641
35-47.40	121-49.72	34.5621	1011.0	CTD 90	71.5	0804-0842
35-42.40	122-00.31	52.7912	1010.0	CTD 91	71.5	1000-1035
35-37.34	122-10.95	71.2838	1016.0	CTD 92	71.5	1154-1230
35-32.33	122-21.48	89.6665	1012.0	CTD 93	71.5	1357-1439
35-27.30	122-32.06	108.1926	1012.0	CTD 94	71.5	1545-1623
36-23.54	122-01.09	12.3921	508.0	CTD 95	68.5	2010-2031
36-18.34	122-11.70	30.7747	854.0	CTD 96	68.5	2139-2211
36-13.49	122-22.23	49.0935	1012.0	CTD 97	68.5	2318-2359
36-08.63	122-32.08	67.5653	1010.0	CTD 98	68.5	0108-0147
36-03.48	122-43.68	86.0787	1012.0	CTD 99	68.5	0252-0328
35-58.54	122-54.32	104.4808	1012.0	CTD 100	68.5	0433-0513
35-53.53	123-05.00	122.9508	1014.0	CTD 101	68.5	0619-0654
35-48.50	123-15.53	141.3378	1012.0	CTD102	68.5	0806-0843
35-43.51	123-26.19	159.8051	1012.0	CTD 103	68.5	0949-1027
35-38.46	123-36.88	178.4407	1012.0	CTD 104	68.5	1138-1222
35-33.39	123-47.41	196.8001	1012.0	CTD 105	68.5	1331-1411
35-17.98	123-36.32	31.0272	1010.0	CTD 106	70	1612-1650
35-22.94	123-25.73	49.5740	1012.0	CTD 107	70	1826-1905
35-27.93	123-15.01	68.0331	1010.1	CTD 108	70	2121-2159
35-32.87	123-04.32	86.1892	1012.0	CTD 109	70	0037-0114
35-37.95	122-53.92	104.9366	1010.2	CTD 110	70	0342-0419
35-42.92	122-43.23	123.3466	1010.0	CTD 111	70	0602-0637
35-48.04	122-32.52	141.7641	1010.4	CTD 112	70	0841-0421
35-52.89	122-21.98	160.1906	1010.0	CTD 113	70	1050-1132
35-57.92	122-11.35	178.8418	1012.0	CTD 114	70	1311-1354
36-02.92	122-00.59	197.3001	1012.0	CTD 115	70	1538-1615
36-31-.97	121-56.61	Time S	278.0	CTD 116	CBTSs	1956-1211
36-31.96	121-56.68	Time S	304.0	CTD 142	CBTSe	2057-2110

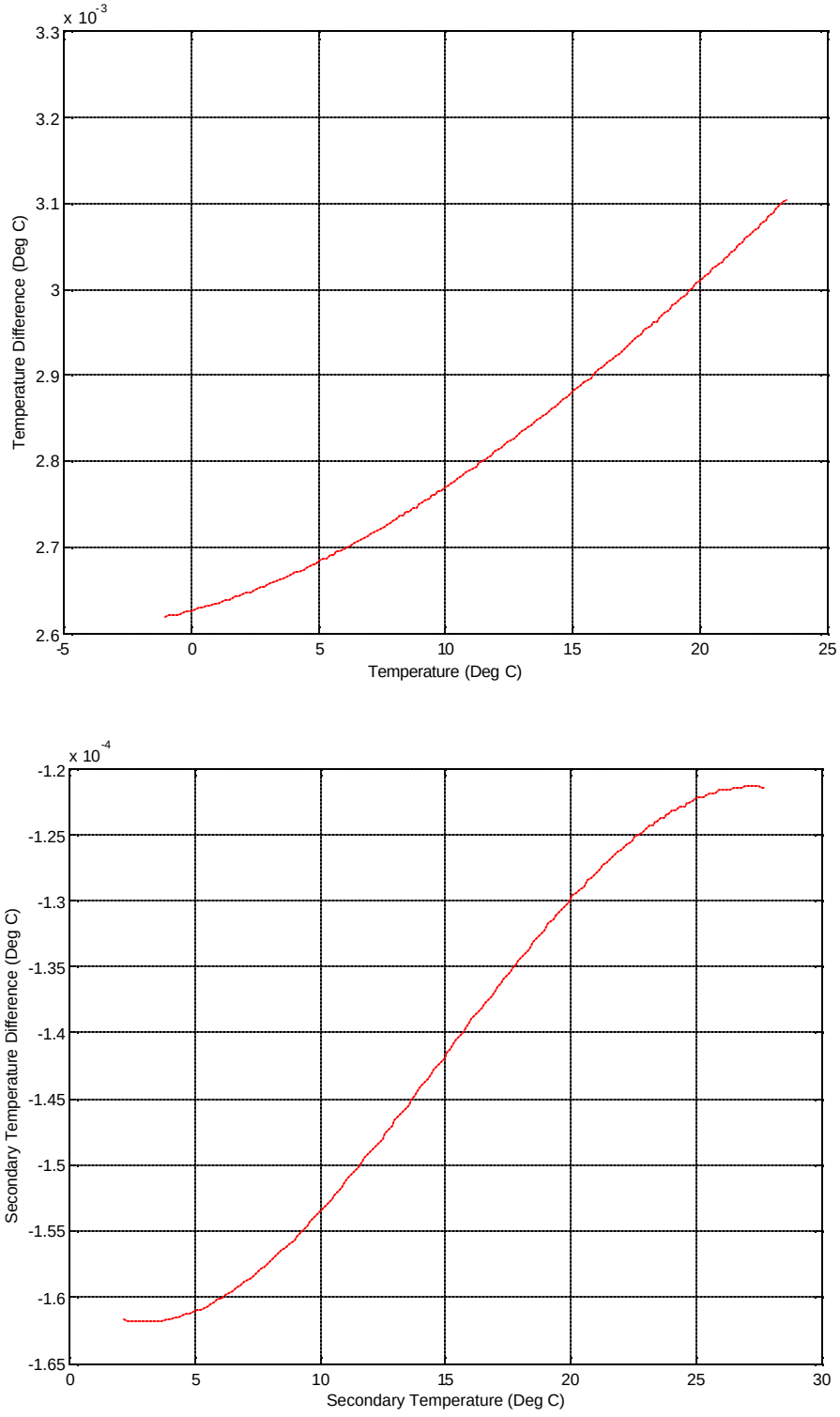

Figure II-1. Temperature difference between pre and post cruise calibration as a function of temperature. (upper) Primary temperature, SeaBird module #2673. (lower) Secondary temperature, SeaBird module # 2631.

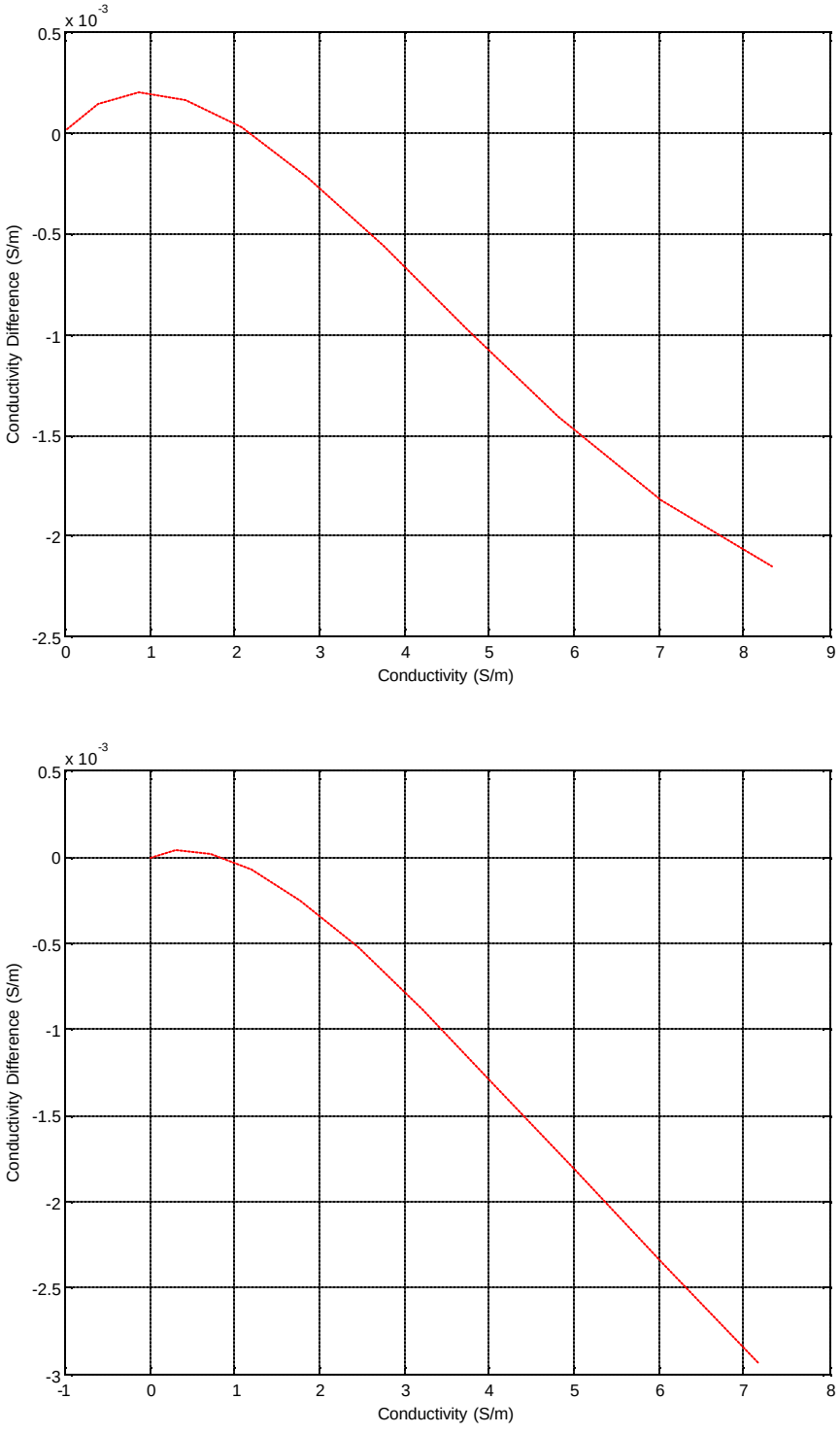

Figure II-2. Conductivity difference between pre and post cruise calibration as a function of conductivity. (upper) Primary conductivity, SeaBird module #395. (lower) Secondary conductivity, SeaBird module #434.

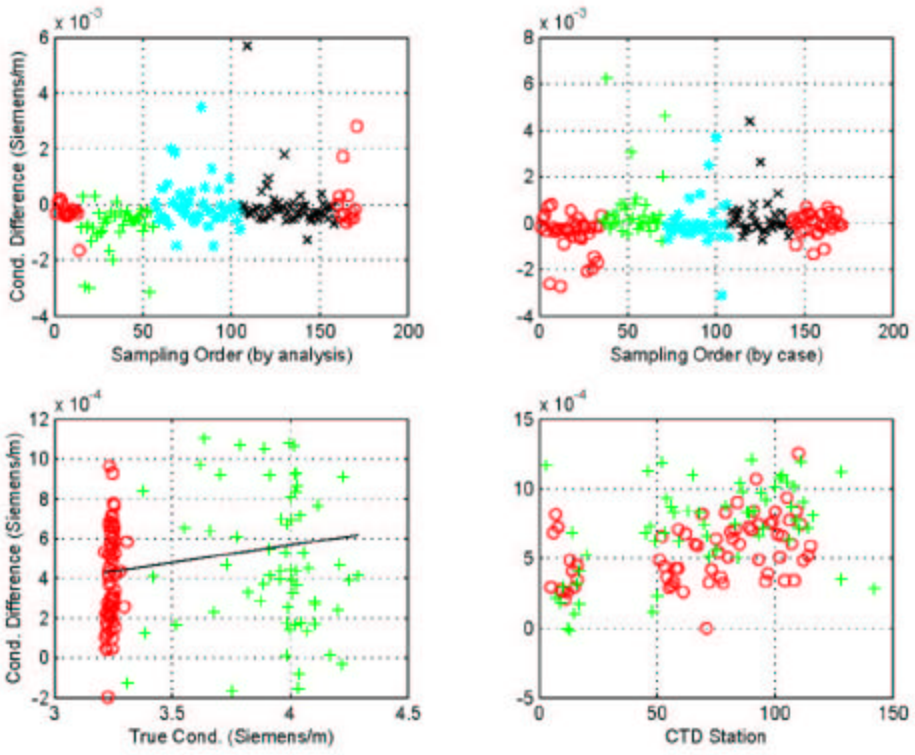

Figure II-3. Post-cruise SeaBird conductivity calibration for SeaBird conductivity sensor #395. (upper left) Bottle sample minus sensor conductivity, plotted in order of analysis. The order of analysis was 3 Dec 02, 4 Dec 02, 5 Dec 02, 9 Dec 02, 10 Dec 02. (upper right) Bottle sample minus sensor conductivity plotted alphabetically by case. The order is C,E,J,Q,M(ixed). (lower left) Bottle sample minus sensor conductivity plotted versus true conductivity by depth. Red circles are "deep" and green crosses are "shallow" where "deep" > 700 dbars. The solid black line shows the linear fit of the least squares based on the slope and offset values (lower right) Bottle sample minus sensor conductivity plotted by CTD station, red circles are "deep" and green crosses are "shallow" where "deep" > 700 dbars.

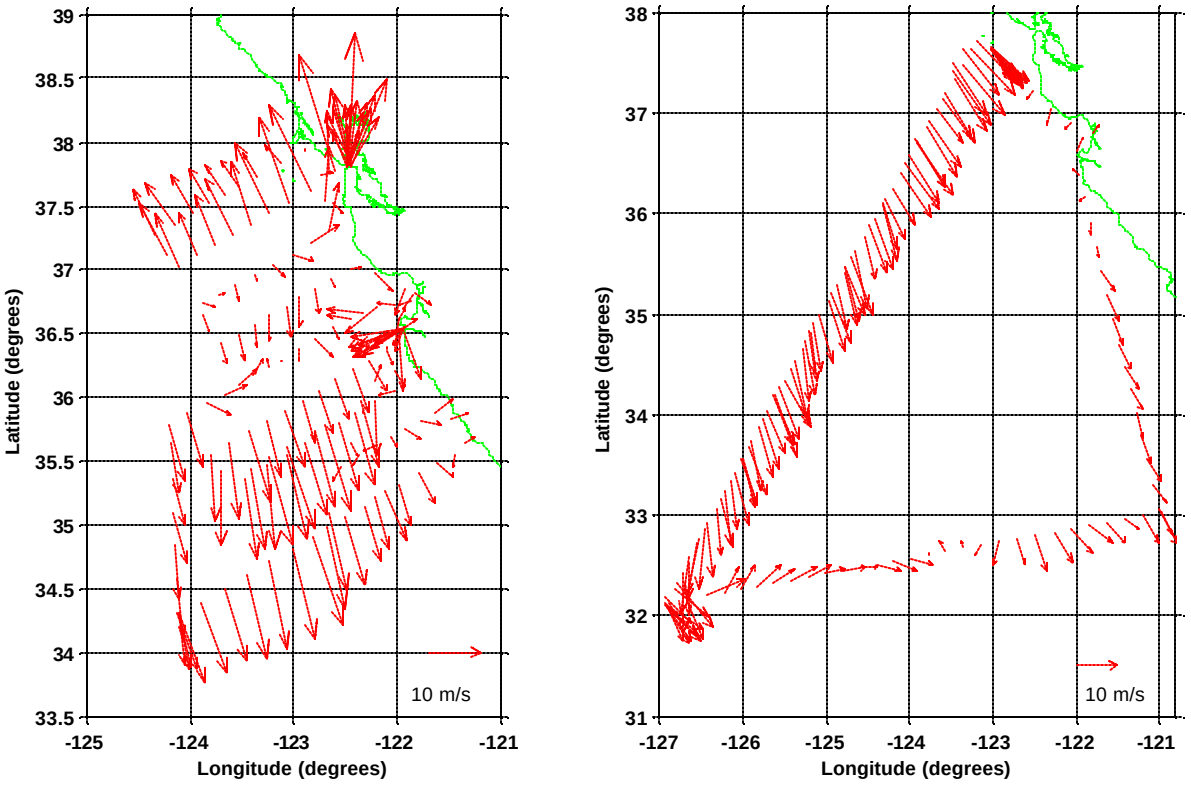

Figure II-4. Underway winds collected by the UDAS system. (left) NAVOCEANO winds 5-19 November 2002. (right) Hoke winds 22-31 October 2002.

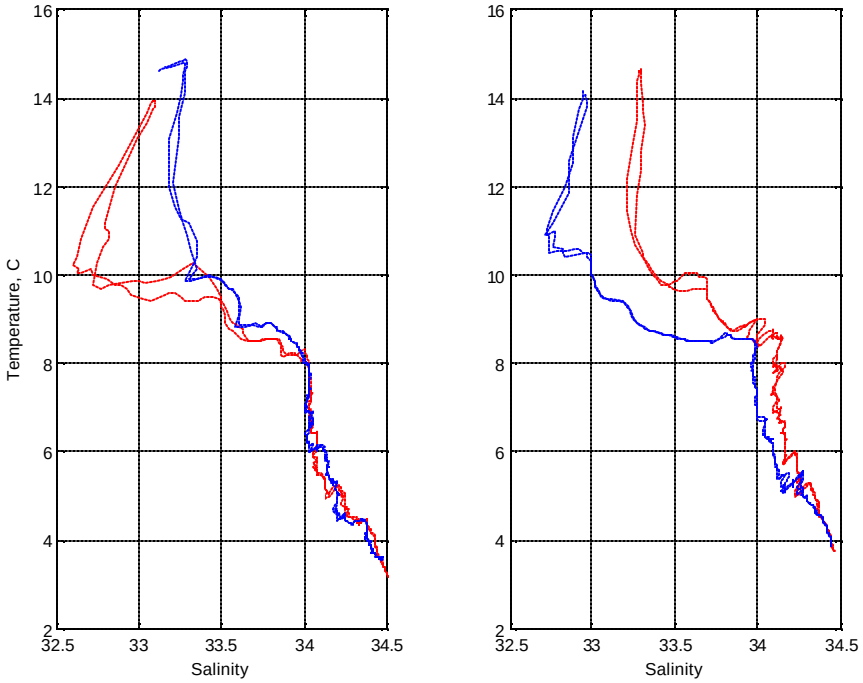

Figure II-5. Temperature-Salinity diagrams for the two stations occupied on both the Hoke and the NAVOCEANO cruises. The blue lines indicate the data from the NAVOCEANO Cencal cruise and the red lines indicate the data from the Hoke Seamount cruise. (left) Station 63-70. (right) Station 61.5-60.

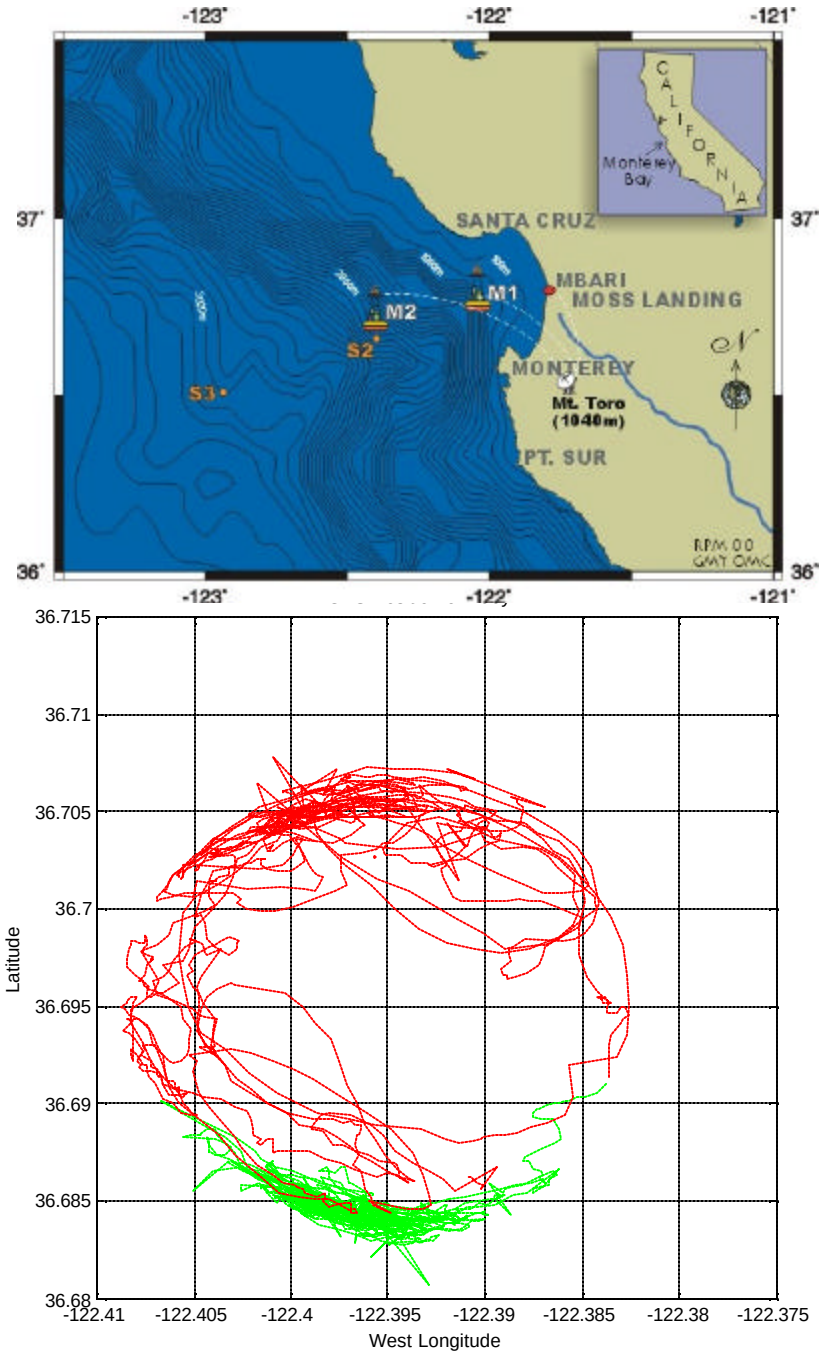

Figure II-6. Data and location of buoy M2 (MBARI, 2003). (upper) Diagram showing the location of buoy M2 (monitored by MBARI and NPS). (lower) shows the GPS position of M2 where the green indicates year day < 305.5 (October) and the red indicates year day >305.5 (November).

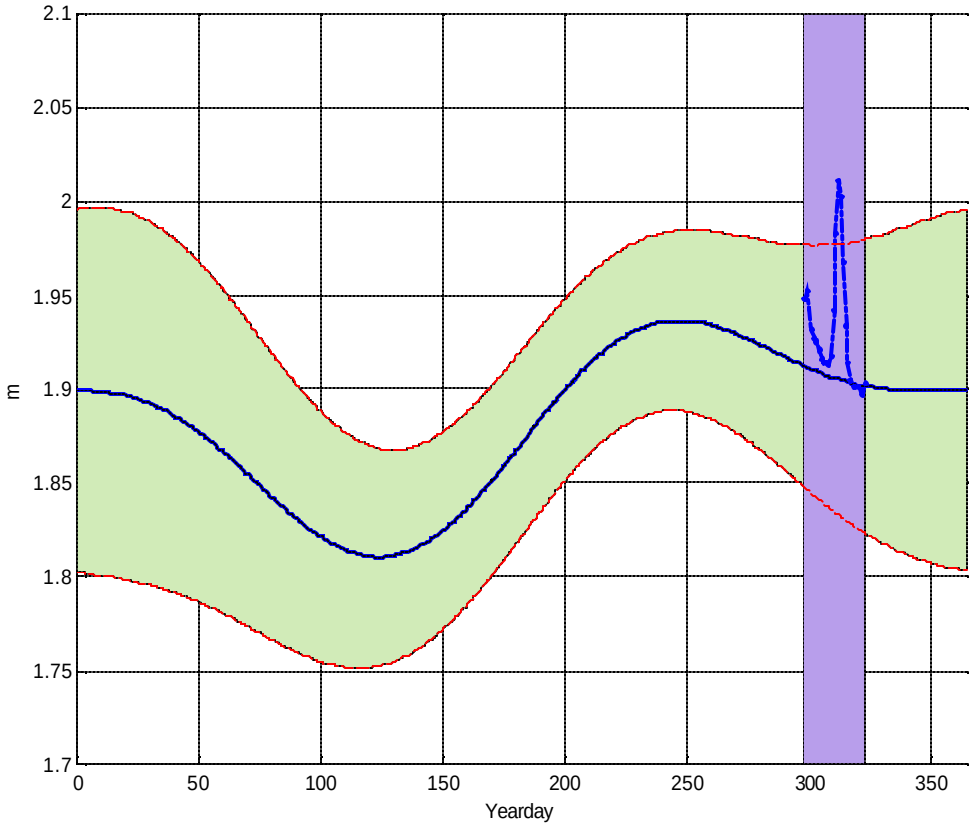

Figure II-7. Annual cycle of daily mean sea level from 1974-2001 (referenced to Mean lower low water) for Monterey, CA. Green shaded area represents plus/minus one standard deviation and the purple shaded area represents the time period of cruises discussed in this thesis (22 Oct-19 Nov 2002). The sea level for 22 Oct-19 Nov 2002 is overlaid in blue.

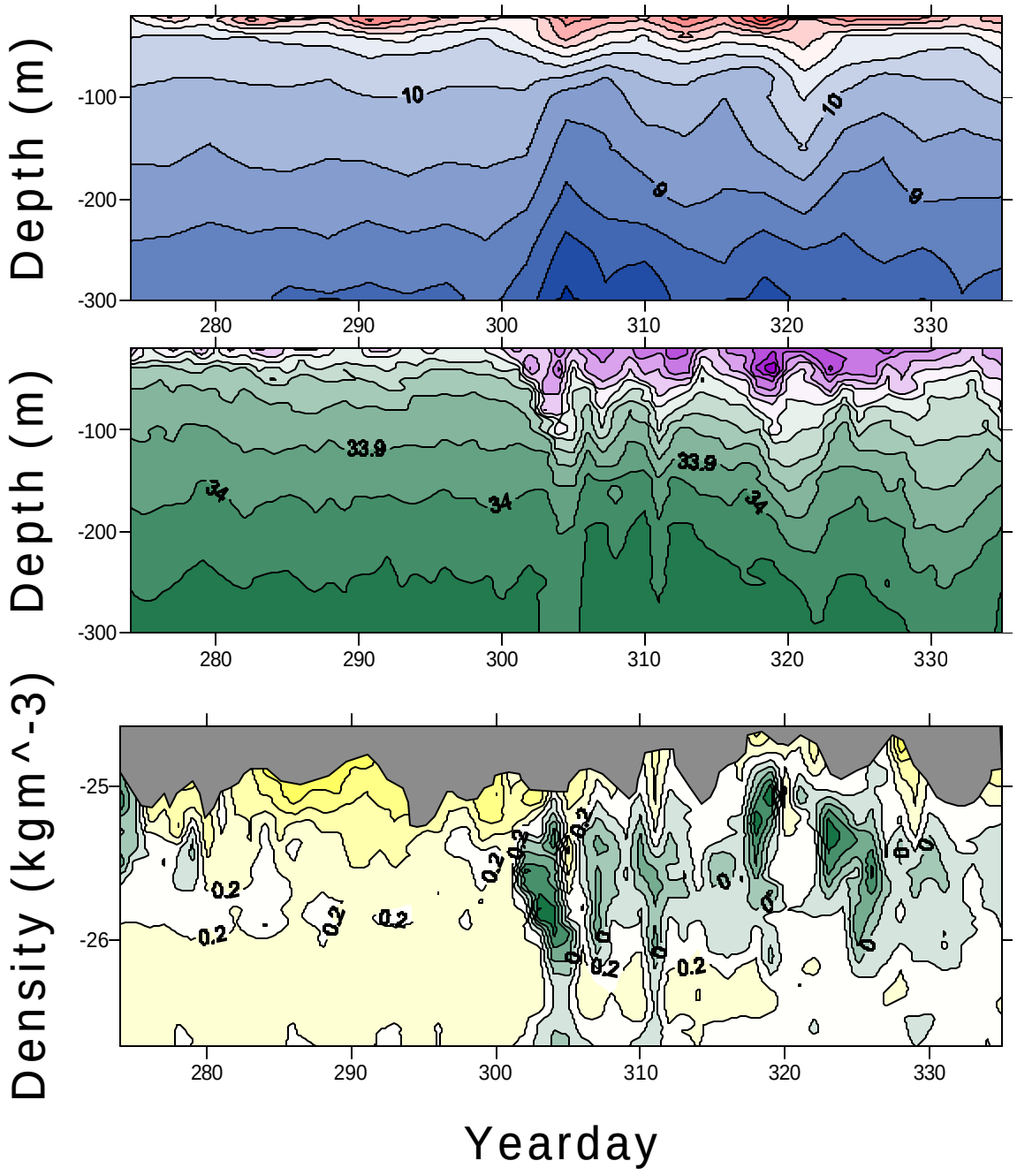

Figure II-8. Water properties at M2 over time (yearday). (top) Temperature (^{o}C) stratification with depth (m). Contour interval is 0.5 ^{o}C. (middle) Salinity stratification with depth (m). Contour interval is 0.1. (bottom) Density anomaly (kg m^{-3}) versus spice (kg m^{-3}). The contour interval is 0.1 kg m^{-3}. The lower limit for the gray region shows the minimum (surface) density anomaly.

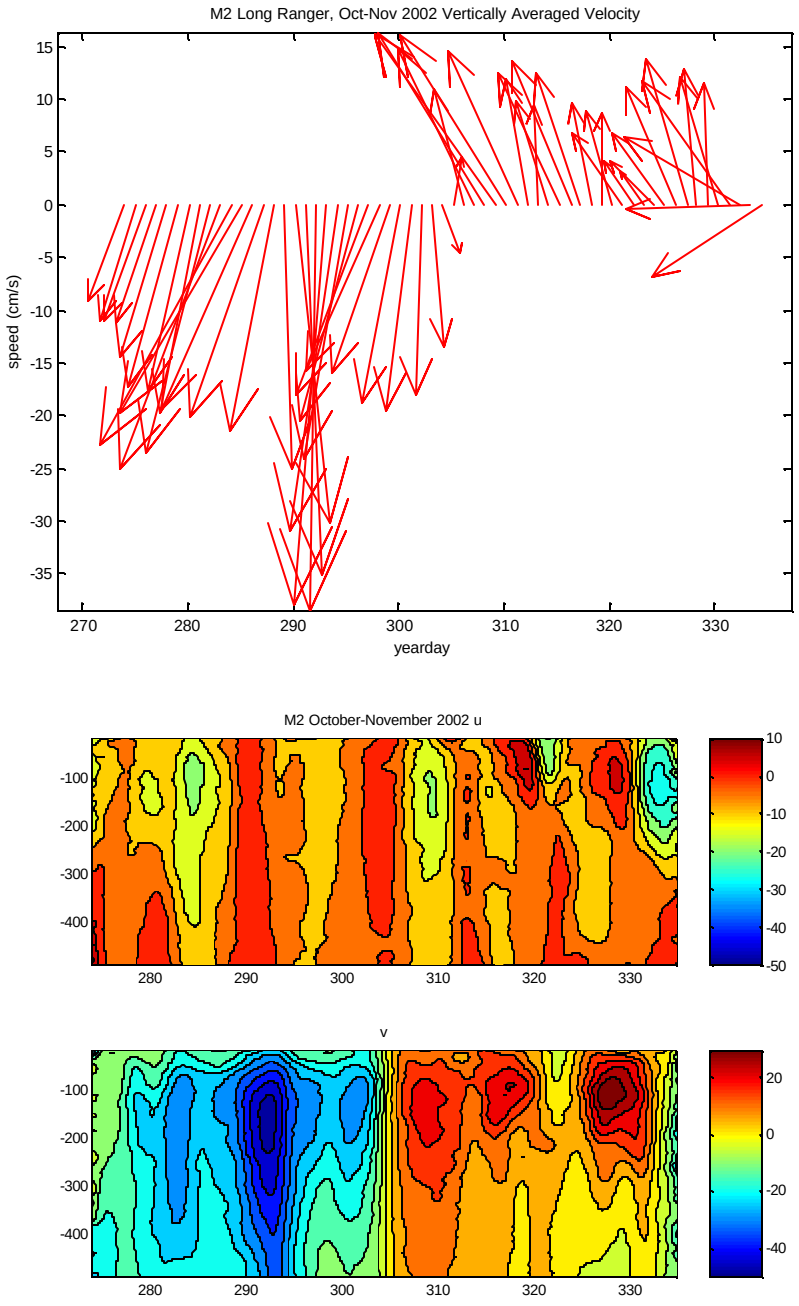

Figure II-9. ADCP data from M2. Data has been smoothed to remove tidal fluctuations (upper) The vertically averaged current velocities at buoy M2 over time. The y-axis shows the magnitude of the velocities in cm/s. (lower) The u and v components of the velocity over time in cm/s.

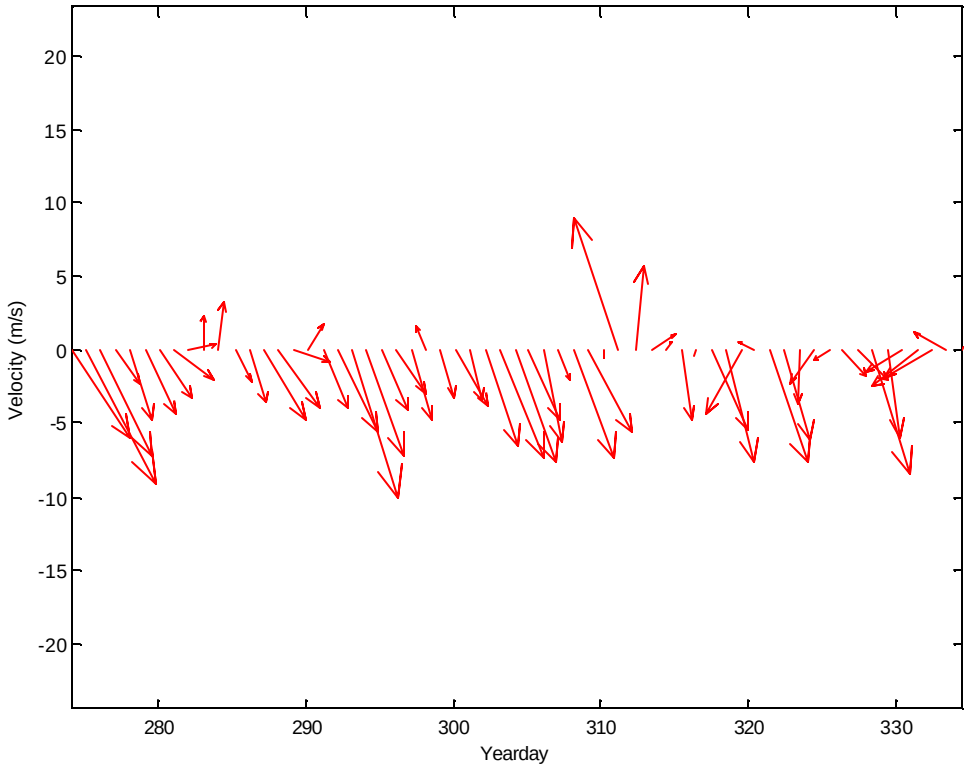

Figure II-10. M2 winds (cm/s), October-November 2002.

THIS PAGE INTENTIONALLY LEFT BLANK

III. RESULTS

Results of the Hoke Seamount cruise are discussed first. These results describe the circulation pattern observed during late October, 2002. Next the properties of the waters associated with the NAVOCEANO cruise are discussed in detail. Following that discussion, isopycnal and isobaric surfaces are analyzed and dynamic thicknesses for several layers presented. Finally, the ADCP data for the cruises are discussed.

A. HOKE SEAMOUNT CRUISE

The Hoke Seamount cruise collected data from 22-31 October 2002 along a section between Hoke Seamount and the Gulf of the Farallones. The section cuts obliquely through the coastal zone, beginning well offshore in the CC. The salinity for the upper 300 m along this section is shown in Fig III-1. Two distinctive low salinity ($S<33.2$) features are clearly seen in Fig. III-1. Both were characterized by a subsurface salinity minimum, S=32.6-32.7, between 50 and 100 dbars. The first occurred at the southern end of the section at 32°N. The second salinity minimum was centered at 35.7°N. These low salinity waters are Subarctic surface waters which are carried southward by the CC and are separated from deeper, saltier waters by the halocline ($33.5<S<34.0$). The region beneath the bottom of the halocline and 300 dbar is relatively uniform, S~34.1.

The southern salinity minimum is characteristic of the seasonal mean southward flow of the CC (Lynn and Simpson 1987), while the salinity minimum in the middle of the section was caused by a meander (this feature will be referred to as a meander although it may be an eddy) of the CC. From 32°N, the halocline sloped upward toward the northeast to 34.5°N. The shoaling of the halocline toward the coast caused an offshore directed horizontal pressure gradient associated with the southward geostrophic flow of the CC. At 34.5°N, sea surface salinity was maximum, S=33.4. The meander occurred immediately to the northeast of the surface salinity maximum and was marked by a U-shaped deepening of the halocline between 35°N and 36.8°N. At 35.8°N, the halocline was almost at the same depth as at 32°N. The southern side of the meander was steeper than the northern side, while the strongest horizontal salinity gradients in the

section were observed between the surface and 180 dbar at 35.1°N. The meander had two cores of S=32.7, one centered at 35.2°N and the other at ~35.8°N. From the northern edge of the meander to the continental shelf, the halocline sloped downward and was about 30 dbar deeper at the edge of the continental shelf (Fig III-1).

Figure III-2 is a chart of the VMADCP measurements, showing the magnitude and direction of the currents observed during the Hoke cruise. The current vectors were averaged over one hour (12 five-minute samples) and vertically from 25 m to 75 m (this includes the 8 m bins at 31, 39, 47, 55, 63, and 71 m). Between Hoke Seamount and 34.5°N, flow was mostly southeastward at 10-30 cms^{-1}, confirming the association of the equatorward flowing CC with the low salinity waters described above. The currents associated with the CC meander were visible from ~35°N to 36.8°N. Velocities of greatest magnitude, about 40 cms^{-1}, occurred over the strong horizontal salinity gradients on the edges of the low salinity intrusion and weakened at the center of the intrusion and outward. The velocity was zero between the two cores of lowest salinity at 35.5°N. North of 35.5°N the flow was onshore (northeastward to eastward), while south of 35.5°N the flow was offshore (northwestward to westward). To the north of the meander over the continental slope to the west of the Gulf of the Farallones, the flow was predominately westward at 10-30 cms^{-1}.

Figure III-3 is a plot of the cross-section (Fig III-3, upper) and along shore section (Fig III-3, lower) velocities for the upper 300 m depth. The zero isotach indicated a change in the flow direction. Although many isotachs were nearly vertical, features in both plots were strongest above 150 m depth. Cross-section velocities (Fig III-3, upper) show a separation of flow regimes at 34.5°N denoted by the zero isotach. South of 34.5°N the velocities associated with the CC were small in magnitude (~0-10 cms^{-1}) and onshore (south and eastward) in direction. North of 34.5°N, the flow was associated with the meander of the CC. With speeds reaching a maximum of approximately 30 cms^{-1} at both low salinity cores, the zero isotach fell between the S~32.7 minima in Figure III-1 and marked the center of the meander at 35.5°N. With an offshore flow between 34.5°N and 35.5°N and an onshore flow between 35.5°N and 36.8°N, the circulation was cyclonic (clockwise). The alternating centers of velocity were indicative of typical flow in and around an eddy or meander.

The along shore section velocities (Fig III-3, lower) were characterized by nearly vertical isotachs and speeds less than 20 cms^{-1} except for the northern half of the meander where the flow above 70 m exceeded 20 cms^{-1} and exceeded 30 cms^{-1} at the surface at 36^oN. This relatively high speed core corresponded to a similar feature for the cross-section velocity (Fig III-3, upper) and was located in the area of the high horizontal salinity gradient at the northern edge of the low salinity intrusion in Fig III-1. For this CC meander region, positive (negative) along shore section velocities tended to align with positive (negative) cross-section velocities. At latitudes less than 34.5^oN, the along shore section flow was positive north of 33^oN (corresponding to the eastward flow of the CC in Fig III-2) and negative father south (corresponding to the southward flow of the CC, Fig III-2).

To summarize Hoke cruise results, a cyclonic meander or eddy of the CC was centered at 36.5^oN. The eddy or meander was about 200 km wide with maximum velocities of 40 cm/s in the upper 75 m and was observed to carry low salinity Subarctic subsurface waters onshore to the north of the meander/eddy center and offshore to the south. The subsequent NAVOCEANO cruise will be used to document the effect of this CC meander/eddy on inshore waters.

B. WATER PROPERTIES

The temperature-salinity (T-S) profile generated for the data from the NAVOCEANO Cencal cruise depicts a T-S profile characteristic of the transition zone of the North Pacific Ocean (Fig III-4, upper) (Dodimead et al., 1963). The halocline marked the division between surface and intermediate waters. Two branches of near-surface water were observed. One was associated with Subarctic surface waters (CC) waters and had a cold halocline around $9\text{-}10^oC$ and a minimum salinity around 32.7. The second branch had a significantly warmer halocline, representing upwelled coastal waters. In addition to the near surface salinity minimum, a salinity minimum related to North Pacific Intermediate waters was observed at some stations in the region beneath the halocline where salinity was nearly uniform (S=34) and $5.5 < T < 7.5^oC$. The final distinctive feature on the T-S diagram extended along 14^oC with $32.2<S<33$. This was data collected in San Francisco Bay.

Spiciness and density provide an alternative view of water properties. Spiciness (π) characterizes water masses and their diffusive stability and has units of kg m^{-3} (Flament 2002). Related to the mixing ratio, spiciness is used primarily to describe the CCS (Lynn and Simpson, 1990; Huyer et al, 2002). Lines of constant spiciness are orthogonal to isopycnals. The highest positive values of spiciness correspond to the warmest and saltiest water; conversely negative values represent the coldest and freshest water. In the spiciness versus density diagram (Fig III-4, lower), regions of water mass variability were better defined. Characteristics become maxima or minima (apparent when the T-S plot is overlaid on lines of constant spiciness and density, Fig III-4, upper).

The salinity minima described in the T-S profile were exaggerated in the spiciness versus density profile (Fig III-4, lower). The near-surface branches of the halocline show clearly in the density and spice diagram: subarctic surface waters with $-0.6 < \pi < -0.4$ kg m^{-3} and upwelled waters with $0.0 < \pi < 0.4$ kg m^{-3}. Both the subsurface salinity minimum associated with Subarctic surface waters and the deeper salinity minimum associated with North Pacific Intermediate water were well defined spice minimums at 25 kg m^{-3} and 26.8 kg m^{-3}, respectively. The waters at the base of the halocline separate these two minima as a spice maximum at 26.4 kg m^{-3}. These three density surfaces, 25, 26.8 and 26.4 kg m^{-3} will be used for isopycnal analysis below.

While the T-S and density-spice diagrams do a good job of characterizing water properties, they do not show the variation of these properties with depth or pressure. Figure III-5 shows the mean and standard deviation of the salinity and spice with pressure for 1000 dbar hydrographic stations. Between the surface and 60 dbars the mean salinity varies minimally around 33.05. Below 60 dbars the halocline occurred, and salinity increased fairly rapidly with depth, from ~33.1 until reaching 34 at 200 dbars. Between 200 dbar and 400 dbar, salinity was relatively uniform, 34.1, subsequently increasing with pressure to 33.3 at 700 dbar and 34.45 at 1000 dbar. At 1000 dbar, the standard deviation of salinity was 0.013, four times the precision of the CTD system.

The mean salinity profile had a subsurface minimum at 50 dbar, while the spice profile showed minima at 60 dbar and 400 dbar. Spice was maximum at the sea surface, while a subsurface spice maximum occurred at 200 dbar. A salinity minimum associated

with North Pacific Intermediate water did not appear on the statistical profiles shown on in Figure III-5.

C. ISOPYCNAL ANALYSIS

Isopycnal surfaces are optimum for following water mass features because horizontal movement and mixing along isopycnals require much less energy and work than diapycnal processes. The "core layer" method of Wüst (Wust and Emery, 1978) can be applied to property distributions to deduce circulation patterns, i.e. the path of the circulation is traced by following the minimum or maximum value of a conservative tracer (Knauss 1997). The shape of the isopycnal surface is represented by isobars that are related to horizontal pressure gradients and can be used to infer the direction and magnitude of geostrophic flow. Here isopycnal analysis is applied to the three water mass features identified above: the salinity minimum associated with the Subarctic surface waters found in the CC eddy at 25 kg m^{-3}, the spice maximum at the base of the halocline at 26.4 kg m^{-3}, and the deep salinity minimum associated with North Pacific Intermediate water (NPIW) and Equatorial waters at 26.8 kg m^{-3}.

Upper layer salinity minimum

In late fall, traces of the high salinity waters that have been upwelled at the coast during spring and summer remain in the upper ocean waters near the coast. Offshore, southward flowing Subarctic surface waters were observed, associated with the CC. The 25.0 kg m^{-3} isopycnal (Fig III-6) upwelled (salinity increased) from a depth of 90 dbar (S~32.75) in the southwest corner of the chart to 5 dbar (S~33.2) along the coast in the Gulf of the Farallones. The 50 to 75 dbar isobars marked a strong pressure gradient at about station 70 on Lines 67-70, while a second distinctive pressure gradient occurred between 10 to 30 dbar near the outer edge of the shelf. For a deep reference level, these pressure gradients imply equatorward geostrophic flow along the isobars. Between these two gradient regions, individual isobars had a complex pattern. For example, the 40 dbar isobar encompassed a trough that extended inshore along Line 67, to the south of Point Sur, and thence offshore along Line 65, as well as surrounding a small trough in the middle of Line 61.5. The salinity makes even clearer the intrusion of the CC waters toward the coast to the north of 36.2°N along 123°W. The 33.05 isohaline connects this

intrusion to lower salinity features (S<32.95) that occurred just south of Point Sur and west of the Gulf of the Farallones along Line 61.5. Note also a tongue of higher salinity water (S~33.2) that extended to the south along the offshore edge of lines 60 and 61.5 and thence inshore along Line 63, wrapping around the northern low salinity feature in a cyclonic manner. To the south, the higher salinity waters, S~33.05, are also intruding between the CC waters offshore and the fresher water south of Point Sur, consistent with an anticyclonic circulation.

The analysis above implies that CC waters were intruding into the coastal zone from the CC meander. As these waters approached the upper slope, they appeared to have flowed both to the northwest and southeast, creating smaller eddies, anticyclonic to the south of Point Sur and cyclonic to the west of the Gulf of the Farallones.

The pressure and salinity of the salinity minimum are investigated in Appendix B and support the above interpretation. On Figure II-6, right, "bull's eyes" appear on the 25.0 kg m^{-3} isopycnal around individual stations in the southeast, suggesting a complex structure for the salinity minimum. Lynn and Simpson (1990) note that this is a signature of mixing processes and use vertical averaging between two isopycnals to get rid of the "bull's eyes". Appendix B used a vertical average of the salinity in the upper 200 dbar as well as an EOF technique to overcome this problem. The result was a reduction in the number of "bull's eyes", however, there were some remaining on the southernmost hydrographic line.

Spice maximum at the base of the halocline

The 26.4 kg m^{-3} isopycnal describes the character of the waters along the base of the thermocline. Although both spice and salinity are charted at this level, note that unlike salinity, spiciness is not correlated with density and was conserved by isentropic motions. (Spiciness can also be used as an indicator of diffusive stability.) The pressure along the 26.4 kg m^{-3} isopycnal (Fig III-7, upper left) shows a distinctive high pressure ridge along the middle of the section which separated poleward flowing waters along the coast from equatorward flowing waters offshore. The height of the ridge ranged from 145 to 180 dbar. The nearshore trough was about 215 to 220 dbar next to the upper slope, while the offshore trough was 240 dbar at the station farthest from shore, i.e.

stations 67-85. Although an offshore pressure minimum (ridge) was observed on each line, 20 dbar valleys ran between the ridge to the north, along Line 67, and to the south. The salinity and spiciness patterns were similar to one another but different than pressure. A core of low spice (0.04) and salt (33.96) ran along the region of large pressure gradient on the offshore side of the pressure ridge which corresponded to the core of the CC meander. This low spice and low salt core penetrated shoreward along Line 67 and thence to the south of Point Sur. The region of high salt and spice was off the continental slope off Año Nuevo (S=33.08, p=0.24) and along the southernmost hydrographic line (S=34.11, p=0.28). To the west of the Gulf of the Farallones, low salt (33.95) and spice (0.08) also occurred but were not connected with similar features to the south.

Deep Salinity Minimum

The density interval, where the contrast between fresher North Pacific Intermediate (NPIW) and saltier Equatorial waters was greatest occurred along the 26.8 kg m^{-3} isopycnal (Fig III-8). Similar to the corresponding features on the 26.4 kg m^{-3} isopycnal, the pressure (Fig III-8, upper left) showed an offshore pressure ridge parallel to the coastline. The isobars deepen both toward the coast (to about 410 dbar) and offshore (to 430 at the station farthest from shore) indicating a circulation pattern consisting of poleward flow near the coast and equatorward flow offshore. The ridge was not as symmetric as the ridge at 26.4 kg m^{-3}. The crest to the northwest extended to 340 dbar while the crest to the southeast was 360 dbar (the difference at 26.4 kg m^{-3} was only 10 dbar). As at the shallower surface, a valley along Line 67 divided the two ridge peaks. The effect of the stronger ridge to the north was to direct more of the low spice (-0.16 kg m^{-3}) and low salt (34.04) water found in the core of the CC eddy to the north. At this level, the southern region of low spice (-0.2 kg m^{-3}) and low salinity (34.03) appeared isolated from the CC by a tongue of higher spice (-0.1 kg m^{-3}) and salt (34.09) water. This tongue originated off Año Nuevo and extended to the south, joining the high salinity water along the southernmost hydrographic line (Line 73).

D. ISOBARIC ANALYSIS

The patterns of temperature, salinity, density and spice are presented for the 2, 200 and 1000 dbar surfaces. The 2-dbar surface interacted freely with the atmosphere

during the period of the cruise so that properties at this level could be affected by air-sea interaction processes, vertical mixing, as well as by advection due to ocean currents (Fig III-9). Well-mixed surface layers were observed to extend to 14.4 dbar during the cruise. Temperatures at 2 dbar (Fig III-9, upper left) were warmest offshore, 17^{o}C, along the axis of flow around the CC meander. These waters were also the freshest (S<32.85), least dense (24.0 kg m^{-3}), and despite the low salinity, highest spice (0.85 kg m^{-3}). In contrast, waters along the continental shelf were colder (<13.2°C), saltier (33.15) denser (24.9 kg m^{-3}) and lower spice (0.3 kg m^{-3}) except near the entrance to San Francisco Bay where waters were fresher, warmer and lighter than those found elsewhere on the shelf. Regions of high salinity, S>33.15) were also found offshore along the most northern and southern lines of the survey. The surface waters also showed the intrusion of fresher, warmer, lighter and spicier CC waters along 123^{o}W toward the continental shelf seen in the isopycnal analyses. The cyclonic eddy to the northwest and the anticyclonic eddy seen south of Point Sur on the 25.0 kg m^{-3} isopycnal are more difficult to discern on the 2 dbar surface although the surface salinity (Fig. III-9, upper right) shows some hints of these patterns.

Properties on the 200-dbar surface were similar to those on the 26.4 kg m^{-3} isopycnal (Fig. III-10). Cold temperatures (<8.2^{o}C) corresponded to the ridge along the 26.4 kg m^{-3} isopycnal, with warmer waters inshore along the upper slope (>9^{o}C) and offshore along the axis of the CC meander as well as along the northernmost and southernmost hydrographic lines (Fig. III-10, upper left). Lobes of coldest water (<8^{o}C) appeared to the north and south, separated by slightly warmer water along Line 67. Horizontal temperature gradients were greatest along the slope and between the two southern hydrographic lines. The CC meander was marked by the fresh water with the freshest water observed at the station farthest from shore (67-85), S<33.80 (Fig. III-10, upper right). Highest salinities were found along the southern hydrographic line, (Line 73) (S=33.12) and off Año Nuevo (S=34.10). The salinity minimum moved from the CC meander along 123°W toward the coast, while patches of lower salinity water (S=34.0) appeared to the south of Point Sur and to the southwest of San Francisco.

Waters on the 200 dbar surface were most dense where the waters were coldest, >26.46 kg m^{-3} (Fig. III-10, lower left). The strongest density gradients occurred along the

upper slope where the eastern boundary waters were <26.38 kg m^{-3} as well as in the area of the CC meander (26.36 kg m^{-3}). Highest spice was found along the southernmost hydrographic line (0.3 kg m^{-3}) as well as along the upper slope from about Año Nuevo to Monterey Bay (0.2 kg m^{-3}) (Fig. III-10, lower right). The lowest spice, -0.08 kg m^{-3}, coincided with the lowest salinity at stations 67-70, but low spice (0.02 kg m^{-3}) also marked the southern portion of the CC meander and the eastern side of the northern cold-water pool.

Where water depth permitted, the 1000-dbar surface was the bottom of our sampling box. The distribution of temperature, salinity, density and spice on this surface are shown in Fig. III-11. Temperature varied from 3.6°C to 4.2°C (Fig. III-11, upper left). Compared with the 200 dbar surface, the region of cold water associated with the upwelling of density surfaces was greatly expanded to the north of Line 67. The upwelling produced the ridge to the south to be much reduced in width, and moved offshore. Warmest waters were observed over the slope off Monterey Bay but waters on the offshore side of the CC meander were also warm, 4.0°C. Salinity ranged from 34.44 to 34.47 (Fig. III-11, upper right). At shallower surfaces, salinity was a useful indicator of water mass (for example, at 200 dbar the inshore waters were derived from equatorial waters and were warm and salty), but at 1000 dbars, salinity variability is mostly controlled by vertical displacements of isopycnals and follows the path shown on the T-S diagram (Fig III-4, upper). Freshest waters (<33.43) occurred to the west of the Gulf of the Farallones and Monterey Bay. The water on the offshore side of the CC was also reduced in salinity, 34.44. The salinity of the colder waters was higher, 34.45, and extended from the northwest to the southeast along the outer portion of the survey region, then onshore at about 35.5°N and north to the west of Point Sur.

If 1000 dbar was a level of no motion, then there would be no variation of density. Figure III-11 (lower left) shows that this is not the case and that density varied from 27.34 kg m^{-3} along the continental slope to 27.4 kg m^{-3} near 36.7°N, 124°W. The region of high density extended to the southeast, indicating that the ridge in the shape of the isopycnals persisted at this depth. Note the valley that separated the northern and southern peaks of this ridge has shifted south of Line 67. The pattern of density variability indicated poleward geostrophic flow along the continental slope as well as

equatorward flow around the CC meander. Spice ranged from -0.12 to -0.17 kg m^{-3} (Fig. III-11, lower right). Highest values occurred along the southern and eastern boundaries, while the lowest value occurred near 37°N, 123.5°W. The pattern of spiciness variability was unique and best fit the temperature chart for this pressure (Fig III-11, upper right).

E. DYNAMIC HEIGHT

The geopotential for three layers (0-200 dbars, 200-500 dbars, and 500-1000 dbars) as well as for the entire water column (0-1000 dbars) is shown in Fig. III-12. Contours of constant geopotential are called isosteres and are streamlines for geostrophic flow. The strength of the geostrophic flow is inversely proportional to the distance between isosteres and the direction of the flow is along the isostere so that values of larger geopotential are to the right of the direction of flow. The strength of the geostrophic flow $|v_g|$ in m/s is given by $|v_g| = \Delta\Phi/(f\Delta x)$, where $\Delta\Phi$ is the geopotential difference, Δx is the distance in meters over which the geopotential difference is determined, and f is the Coriolis parameter. At 36°N and for a contour interval of 0.1 J/kg ($\Delta\Phi$), this simplifies to $|v_g| = 1.17 \times 10^3/\Delta x$. This equation has been used to produce the nomogram shown in Fig. III-12 (lower left) for determining the strength of the geostrophic flow from the distance between two adjacent isosteres.

Off central California, the 0-200 dbar layer typically reflects the shoaling of the pycnocline toward the coast with geopotential decreasing and equatorward geostrophic flow. Figure III-12 (upper left) indicated a more complicated pattern. Geopotential was greatest, >9.3 J/kg, in the southwest corner of the survey area on the offshore side of the CC meander. The strongest gradients of geopotential coincided with the core of the CC meander. Inshore of the meander, gradients were weaker and indicated a series of meanders or eddies inshore. The 0-200 dbar layer was thinnest (smallest geopotential, 8.4 J/kg) along the continental slope west of Monterey Bay, near 36.7°N, 123.6°W, and about 100 km southwest of Point Sur. The 8.8 J/kg isostere connected the outer edge of the CC meander with a northward intrusion along 123°W. Cyclonic circulation was shown around the geopotential minimum at 36.7°N, 123.6°W. The 8.8 J/kg ridge along 123°W and the 8.9 J/kg ridge to the west of the Gulf of the Farallones did not appear to

be connected. The ridge along 123°W was also isolated from the fresh water region south of Point Sur by the dynamic trough that ran south along 122.5°W.

The 200-500 dbar layer is used to show the poleward flow along the continental slope associated with the California Undercurent. This layer typically shows a dynamic trough about 100-150 km from the coast that separates the poleward coastal flow from the CC which is located farther from the coast. Figure III-12 upper right, shows the dynamic trough (outlined by the 4.02 J/kg isostere) in this location but with alongshore variations in its strength. The trough was deepest to the north, >4.02 J/kg. The 4.12 J/kg isostere provided a path for CC meander waters to flow toward the coast along the 200 dbar surface. Geopotential was greatest on the offshore side of the CC meander and offshore of Monterey Bay, > 4.32 J/kg. Poleward geostrophic flow occurred along the continental slope to the west of the Gulf of the Farallones, while equatorward flow was observed around the CC meander offshore.

The lowest layer, 500-1000 dbar, is not sampled by the CalCOFI program but analysis of Line 67 sections (Collins et al., 2003) show a thickening of this layer toward the coast. Fig. III-12, lower left, shows the same dynamic trough observed in the 200-500 dbar layer. Geopotential was greatest along the continental slope (> 4.84 J/kg) as well on the offshore side of the CC meander, > 4.84 J/kg, consistent with poleward flow along the slope and equatorward flow around the CC meander. The dynamic trough was lowest in the north near 37°N, 124°W, <4.54 J/kg, and weaker to the southeast so geostrophic flow along the 4.74 J/kg isostere flows northward along 123°W, connecting the meander with the region to west of the Gulf of the Farallones. The pattern of isosteres in the coastal region south of Point Sur had two smaller scale features.

The geopotential for 0-1000 dbar indicates the flow patterns at the surface assuming that the 1000 dbar surface was level. As for 0-200 dbar, largest gradients were associated with the CC meander along the southeast portion of the chart (Fig. III-12, lower right). The largest geopotential occurred on the offshore edge of the meander, >15.0 J/kg. Inshore of the meander, the dynamic trough consisted of two eddy-like features. The eddy to the north was strongest with a minimum of geopotential, 12.6 J/kg, while the one to the south had the lowest geopotential of 13.1 J/kg. Between these two

cyclonic features, a trough occurred, connecting the CC meander along 123°W to poleward coastal flow to the north. Along the coast, the flow at the surface was poleward and appeared to be deflected offshore just north of Monterey Bay. The geopotential gradients at the surface were weak inshore, characteristic of the Davidson Current.

F. VMADCP DATA FOR NAVOCEANO CRUISE

The VMADCP measurements, showing the direction and magnitude of the currents for the NAVOCEANO cruise are presented in Figure III-13. The currents were averaged vertically over one hour from 25 m to 75 m depth (left) and 275 m to 325 m depth (right). In the layer between 25 m and 75 m (left), the currents were larger in magnitude. Inshore, along the coast the flow was predominately poleward. Offshore between 124.5°W and 122°W, and 34°N and 36°N, the flow was cyclonic (clockwise), associated with the CC meander/eddy. Along 124°W, north of 35°N the currents were predominately onshore (southeastward to eastward). South of 35°N the currents were offshore (westward to southwestward). Velocities of greatest magnitude, about 50 cm/s occurred on the onshore (eastern) side of the eddy/meander. East of 124°W the currents were eastward to southeastward. North of Line 67 the currents were smaller in magnitude (~10-30 cm/s) and north to northeastward in direction. South of Line 67, the flow was more complex. Immediately east of the eddy/meander, the currents were small in magnitude (~0-10 cm/s) and then increased (~30 cm/s). From the meander/eddy, eastward to the coast, the flow was predominately north to northeastward.

For the layer from 275 m to 325 m, the velocities were considerably smaller in magnitude, ranging from about 0 cm/s to about 40 cm/s. The velocities of smallest magnitude occurred just outside the mouth of Monterey Bay along Line 67 and north of Line 67, along Line 63 and 61.5, offshore. East of 123°W, the currents were primarily north to northwest in direction. West of 123°W the cyclonic circulation pattern, associated with the eddy/meander, can be seen clearly. Along 124°W the velocities were greater in magnitude than they were between 25 m and 75 m depth, while the directions were similar. East of 124°W the contrary was true, with the magnitudes of the velocities smaller than they were in the layer between 25 m and 75 m depth.

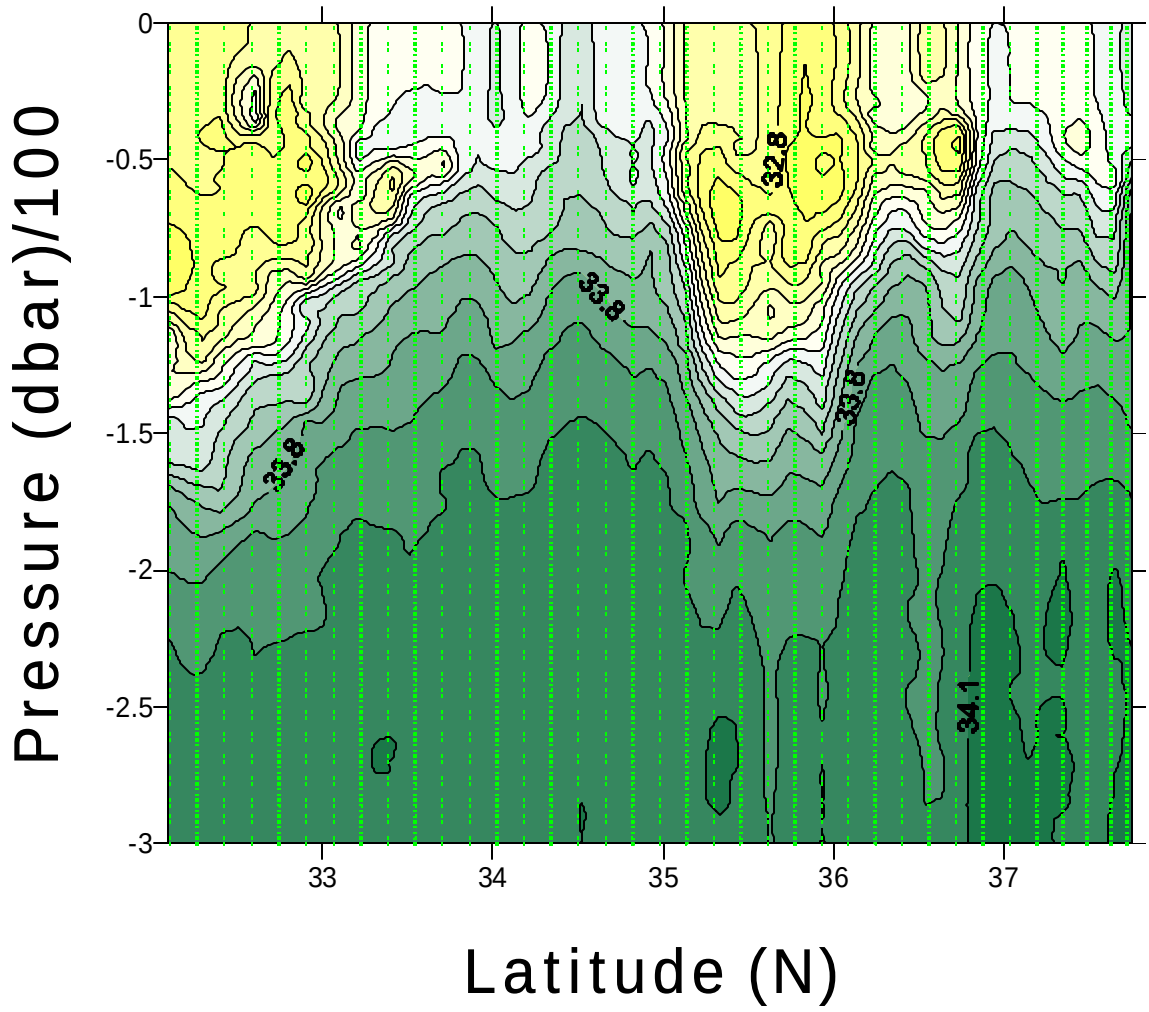

Figure III-1. Hoke to Pioneer Seamount salinity, contour interval is 0.1.

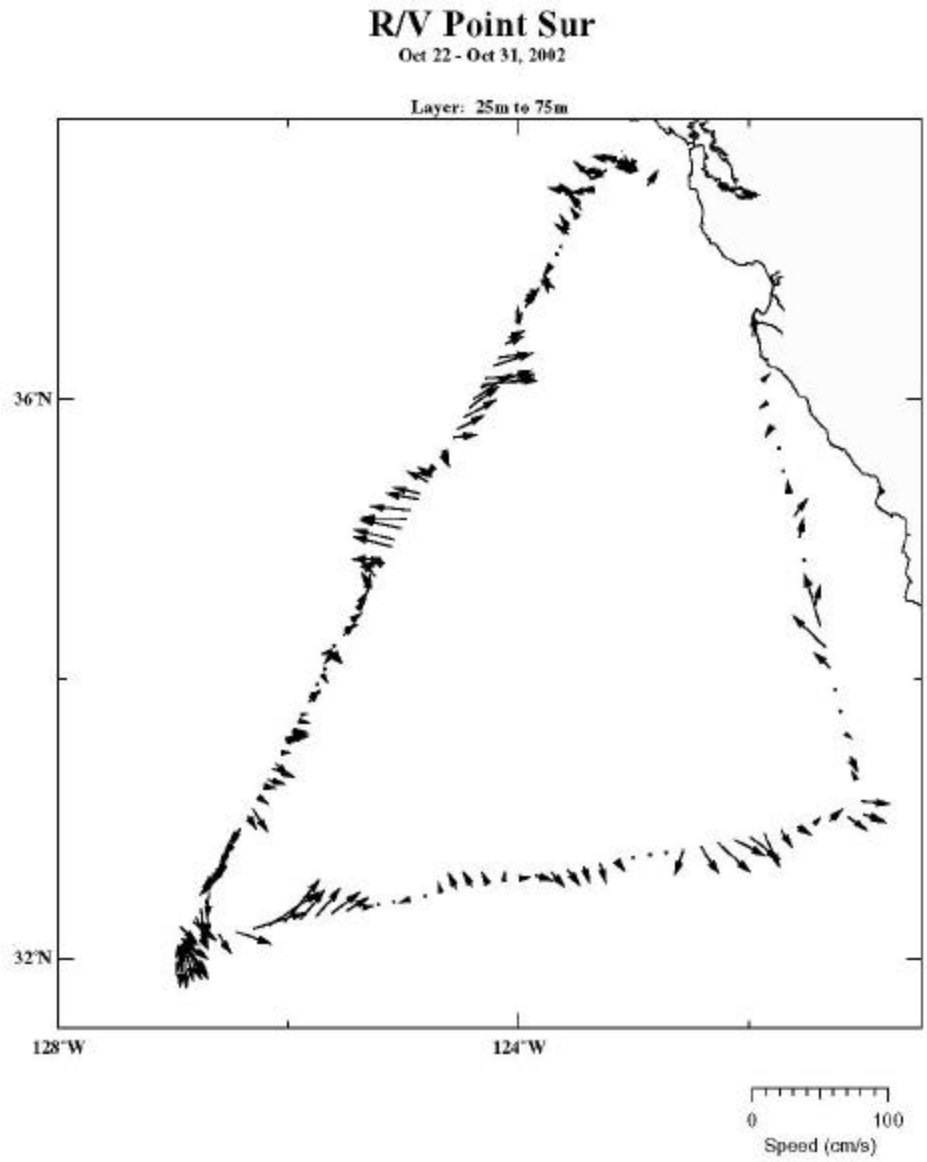

Figure III-2. Hourly averaged ocean currents at a depth of 50 m, 22-31 October 2002. Measurements were vertically averaged from 25 m to 75 m. Arrows indicate magnitude and direction..

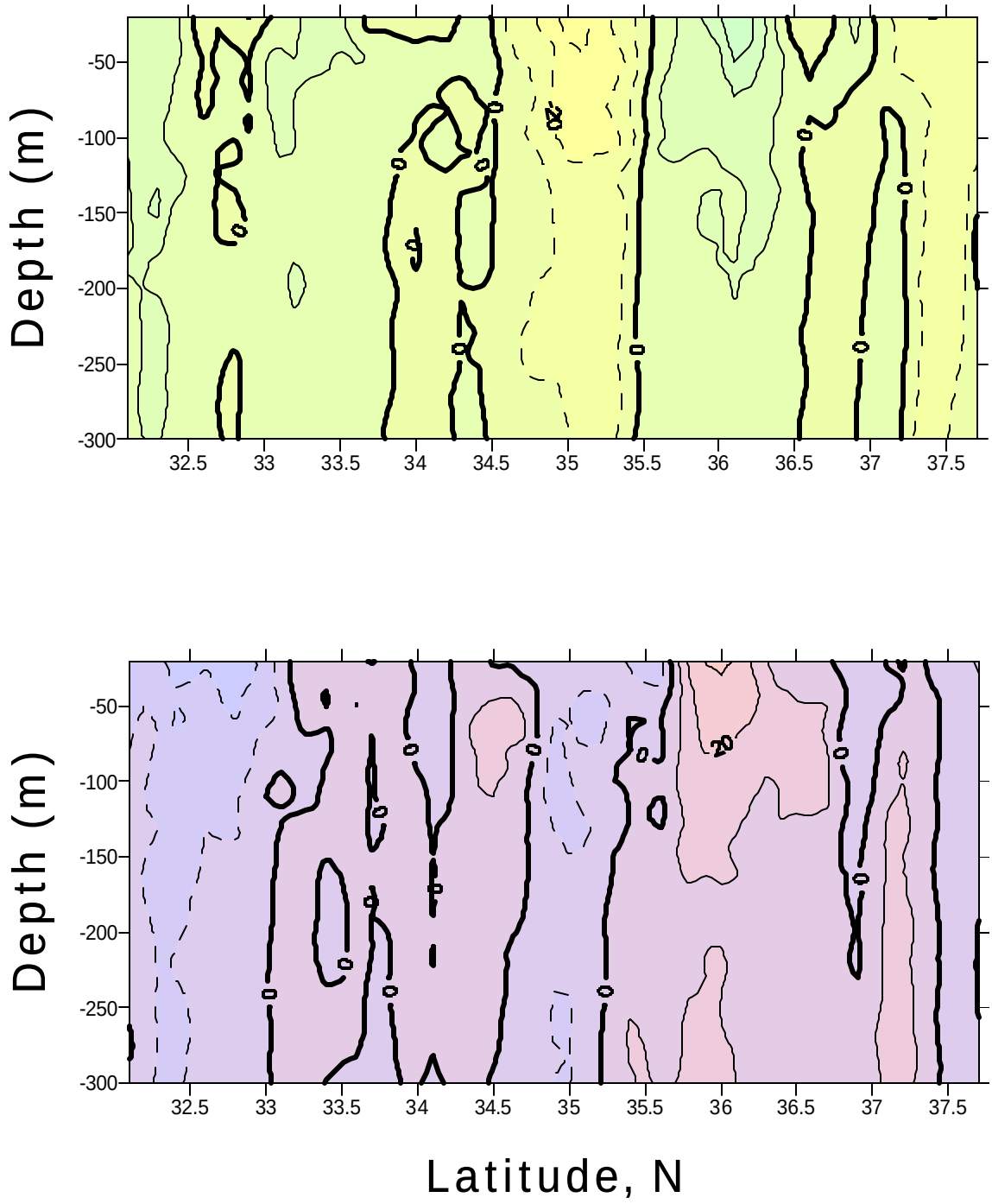

Figure III-3. Upper ocean current velocities from Hoke to Pioneer Seamount. Velocities were averaged over one hour. (top) Cross-section velocity, cm/s; contour interval is 10 cm/s. (bottom) Alongshore section velocity, cm/s; contour interval is 10 cm/s.

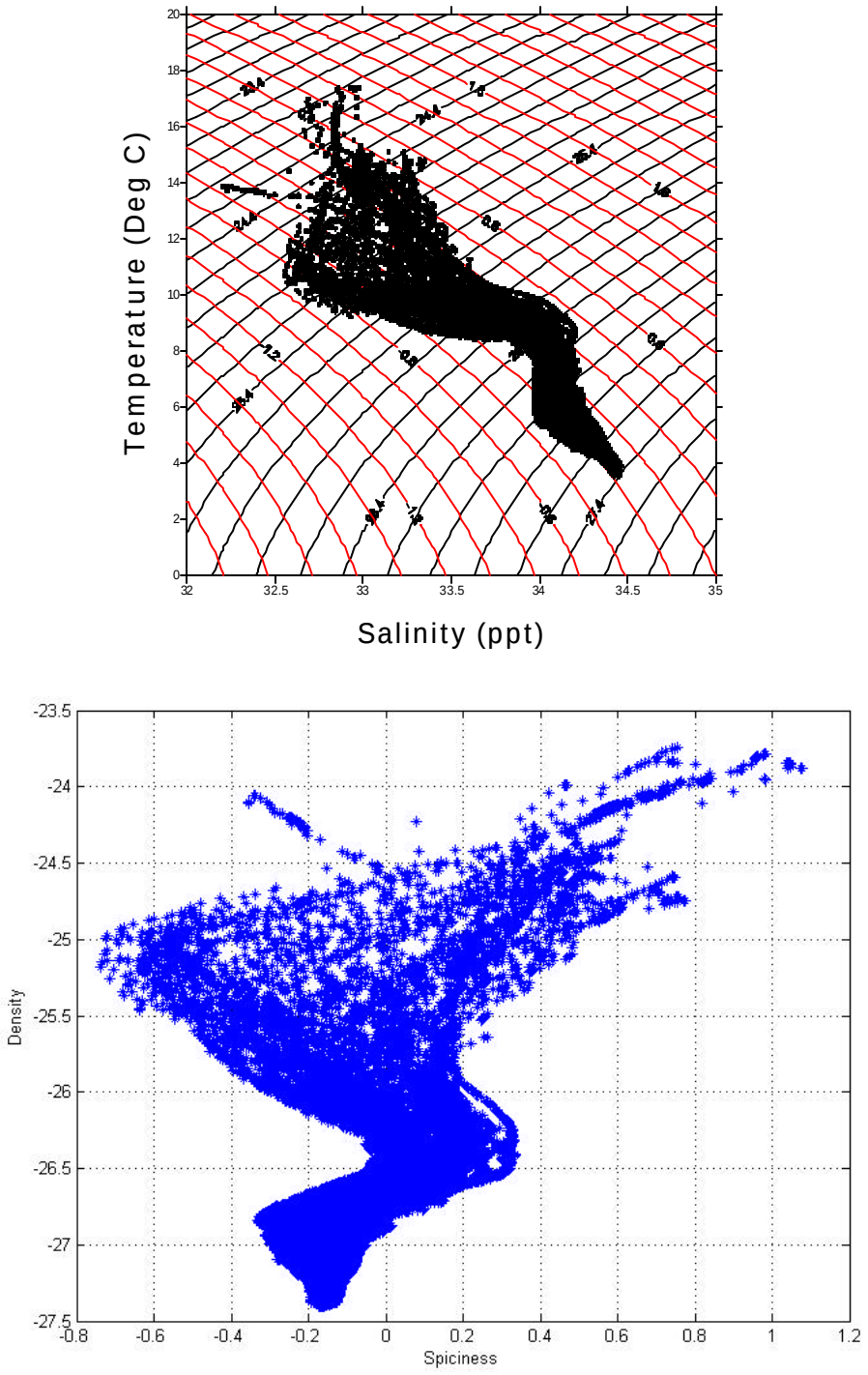

Figure III-4. Water properties for NAVOCEANO Cencal cruise. The line extending from the density values of –24.5 to –24, and along 14°C corresponds to San Francisco Bay water. (upper) T-S diagram, lines of constant density and spiciness are overlaid. Lines of constant spice are red and lines of constant density are black. The contour intervals are 0.2 kg m^{-3}. (lower) Spiciness versus density.

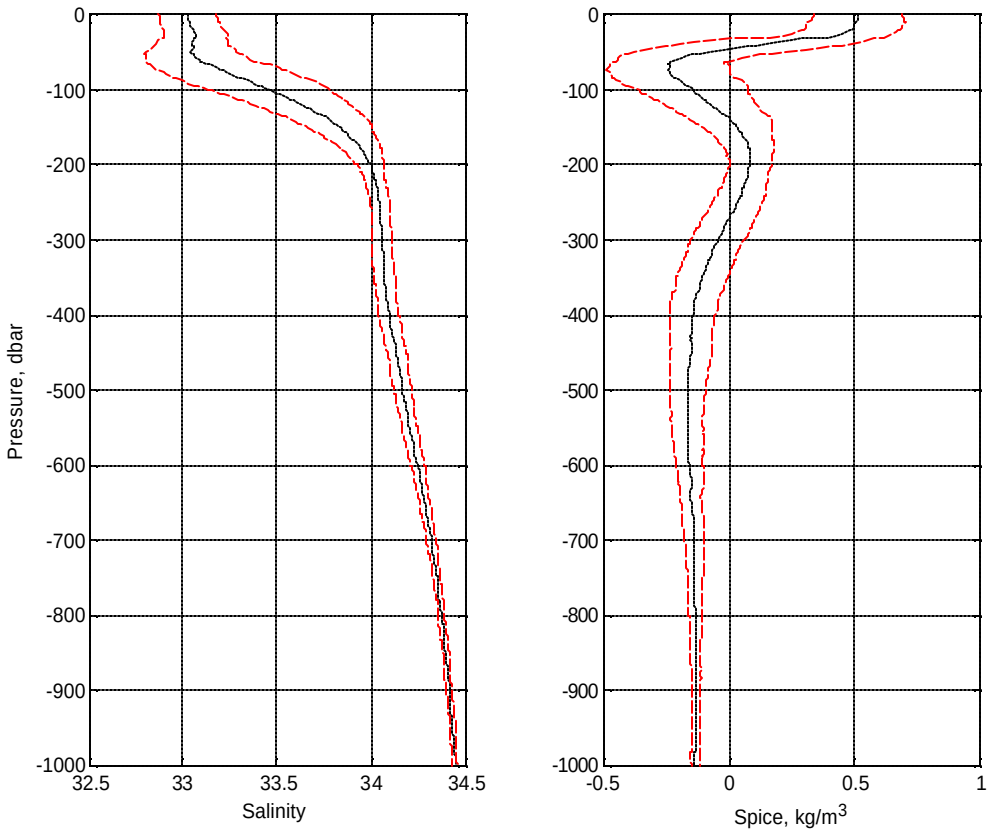

Figure III-5. Vertical profiles. (left) Mean salinity (black line) ± one standard deviation. (red lines). (right) Mean spice (black line) ± one standard deviation (red lines).

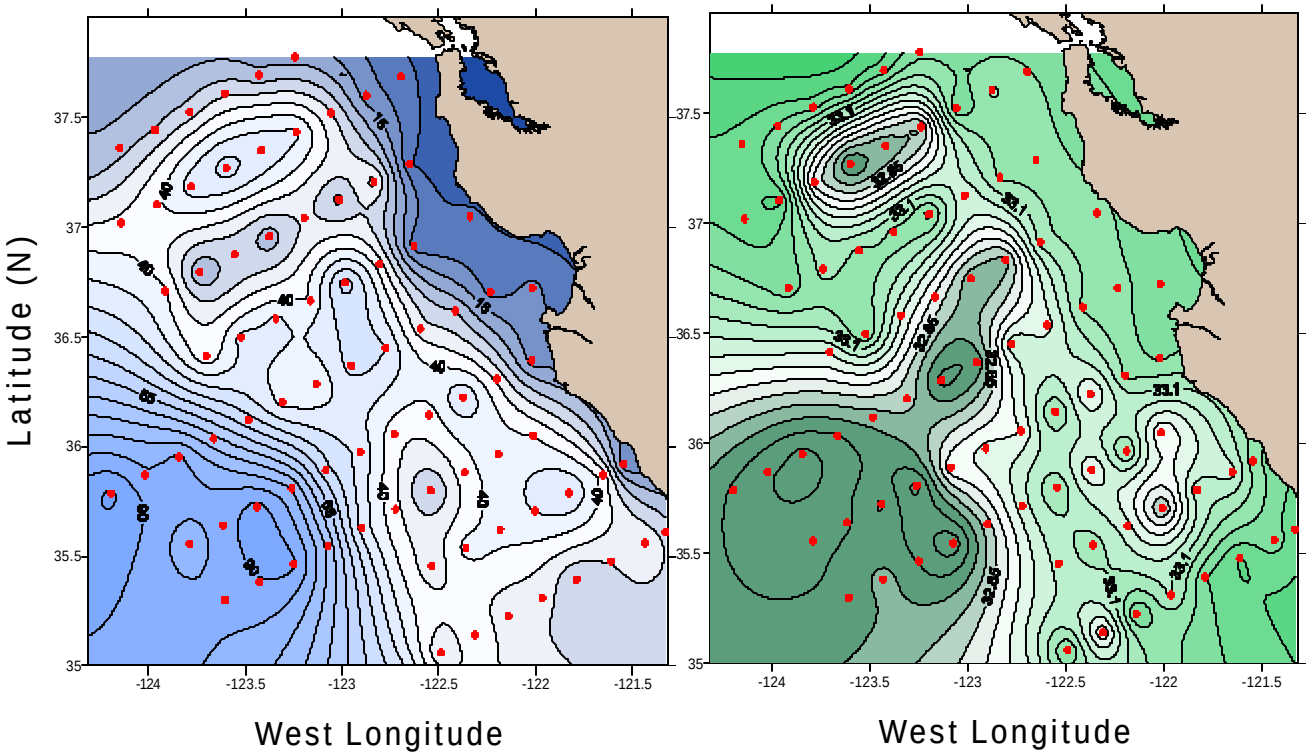

Figure III-6. Properties on isopycnal 25.0 kg m^{-3}. (left) Pressure, contour interval is 5 dbars .(right) Salinity, contour interval is 0.05.

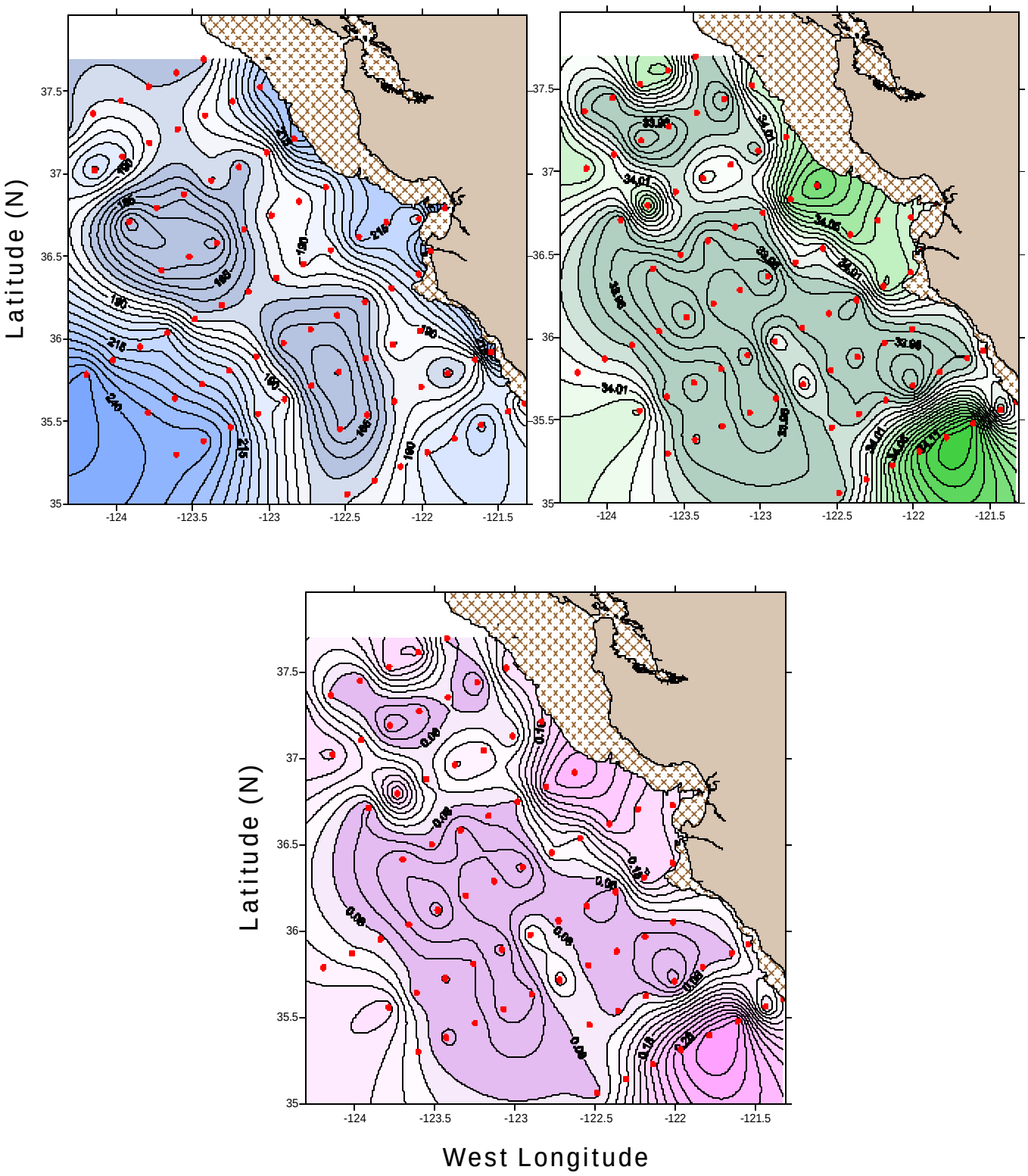

Figure III-7. Properies on the 26.4 kg m^{-3} isopycnal. The 200 m isobath is overlaid. (upper left) Pressure, dbars. The contour interval is 5 dbars. (upper right) Salinity. The contour interval is 0.01. (lower) Spiciness, kg m^{-3}. Contour interval is 0.02 kg m^{-3}.

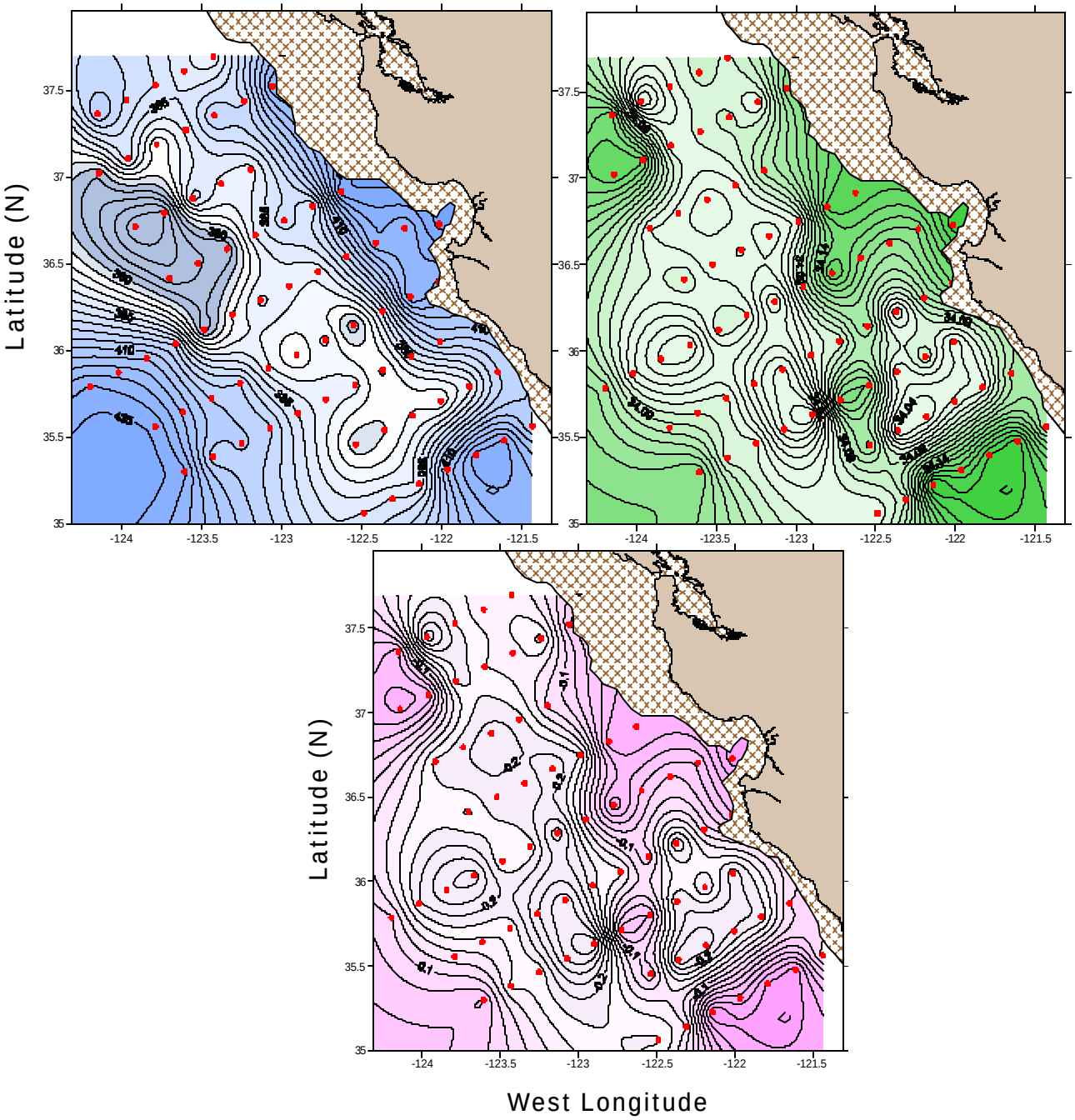

Figure III-8. Properties on the 26.8 kg m^{-3} isopycnal. The 400 m isobath is shown. (upper left) Pressure, dbar. Contour interval is 5 dbars. (upper right) Salinity. Contour interval is 0.01. (lower) Spiciness, kg m^{-3}. Contour interval is 0.02 kg m^{-3}.

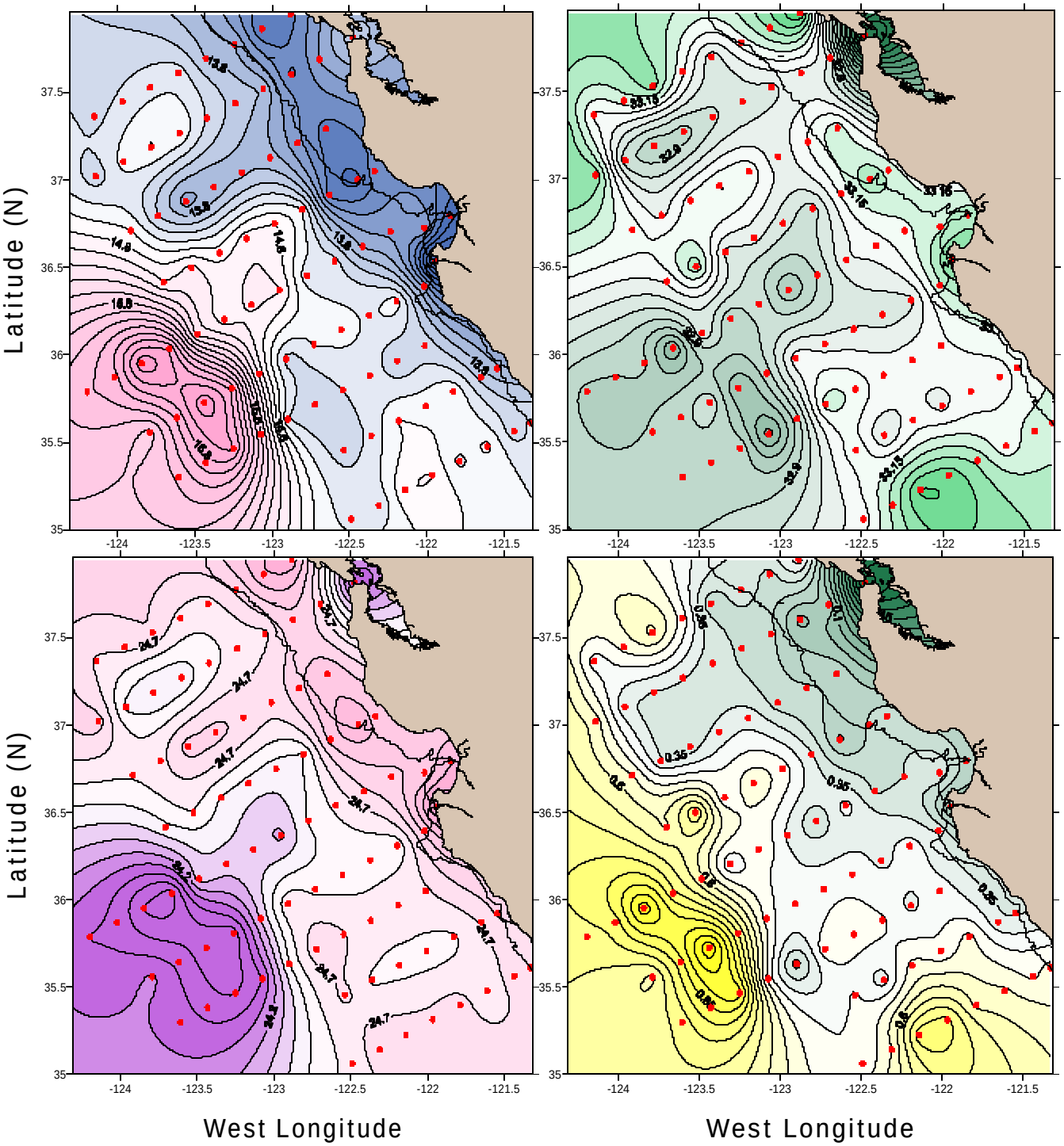

Figure III-9. Properties on the 2 dbar surface. The 200 m isobath is shown. (upper left) Temperature, °C. Contour interval is 0.2°C. (upper right) Salinity. Contour interval is 0.05. (lower left) Density, kg m^{-3}. Contour interval is 0.1 kg m^{-3}. (lower right) Spice, kg m^{-3}. Contour interval is 0.05 kg m^{-3}.

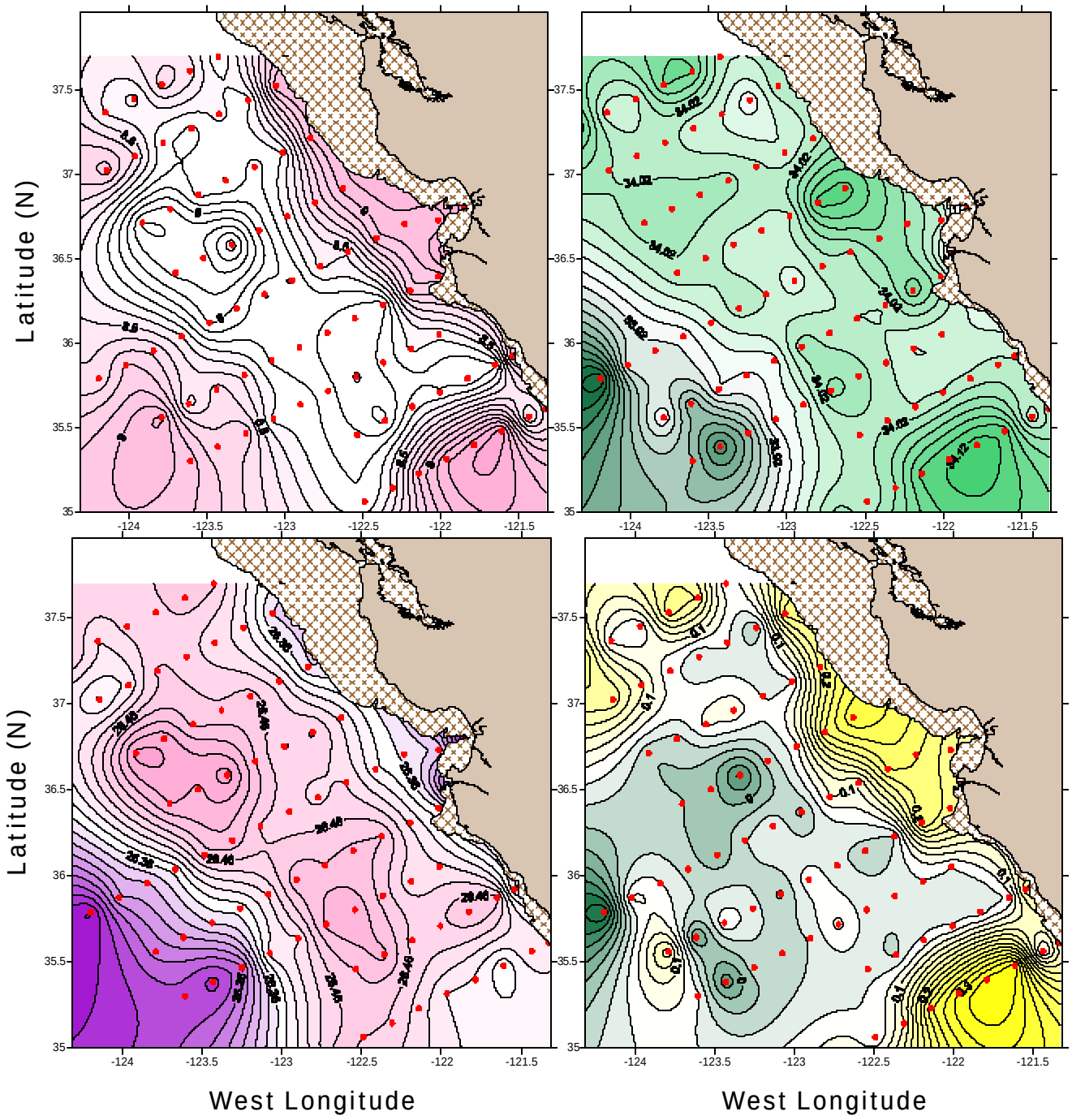

Figure III-10. Properties on the 200 dbar surface. The 200 m isobath is shown. (upper left) Temperature, °C. Contour interval is 0.1°C. (upper right) Salinity, contour interval is 0.02. (lower left) Density, kg m^{-3}. Contour interval is 0.02 kg m^{-3}. (lower right) Spice, kg m^{-3}. Contour interval is 0.02 kg m^{-3}.

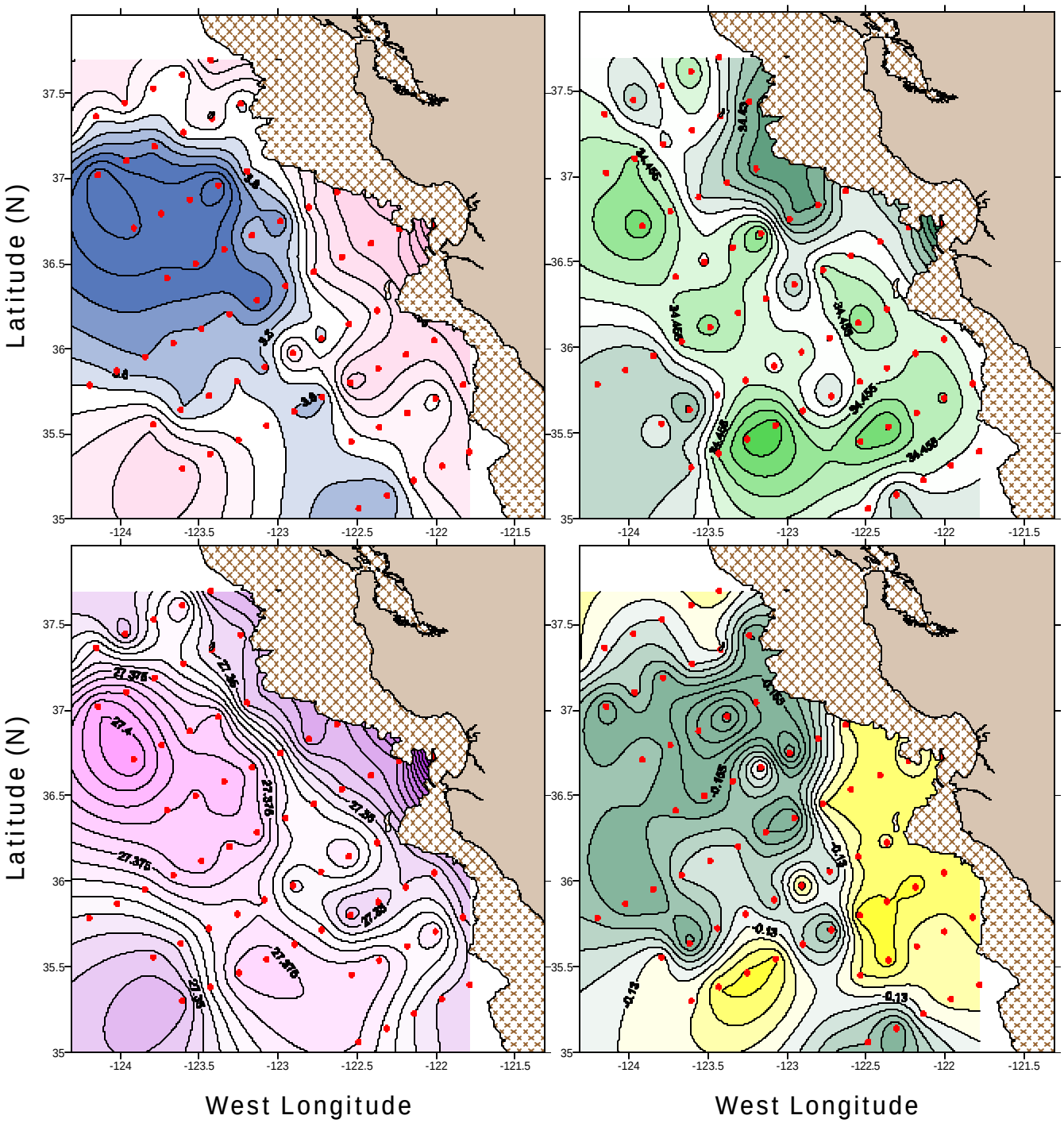

Figure III-11. Properties on the 1000 dbar surface. The 1000 m isobath is shown. (upper left) Temperature, °C. Contour interval is 0.05°C. (upper right) Salinity. Contour interval is 0.005. (lower left) Density, kg m^{-3}. Contour interval is 0.005 kg m^{-3}. (lower right) Spice, kg m^{-3}. Contour interval is 0.005 kg m^{-3}.

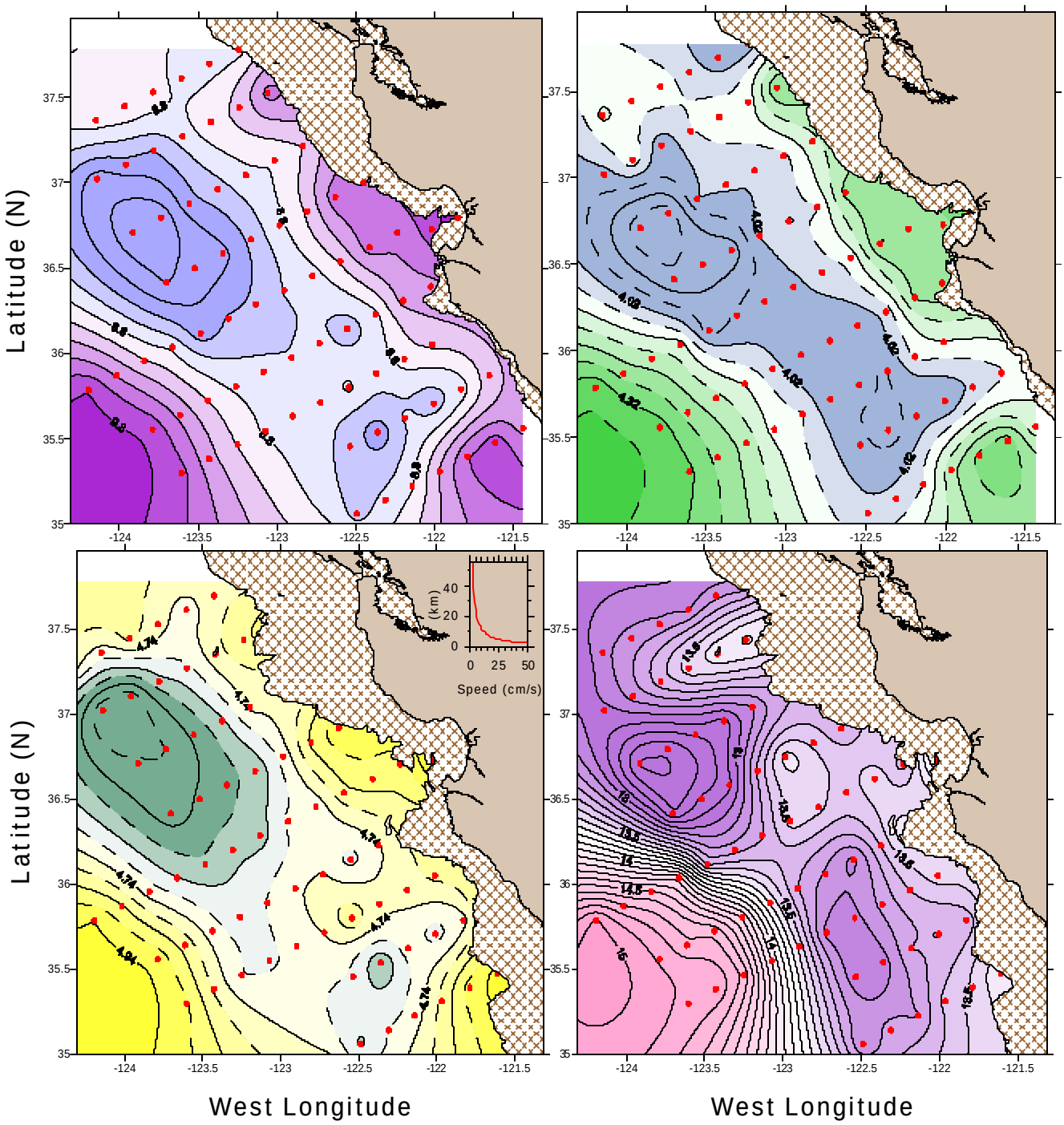

Figure III-12. Geopotential, Joules/kg. (upper left) 0/200, contour interval is 0.1 Joules/kg. The 200 m isobath is overlaid. (upper right) 200/500, contour interval is 0.1 Joules/kg. The 1000m isobath is overlaid. (lower left) 500/1000, contour interval is 0.1 Joules/kg. The 1000m isobath is overlaid. (lower right) 0/1000, contour interval is 0.1 Joules/kg. The 1000m isobath is overlaid.

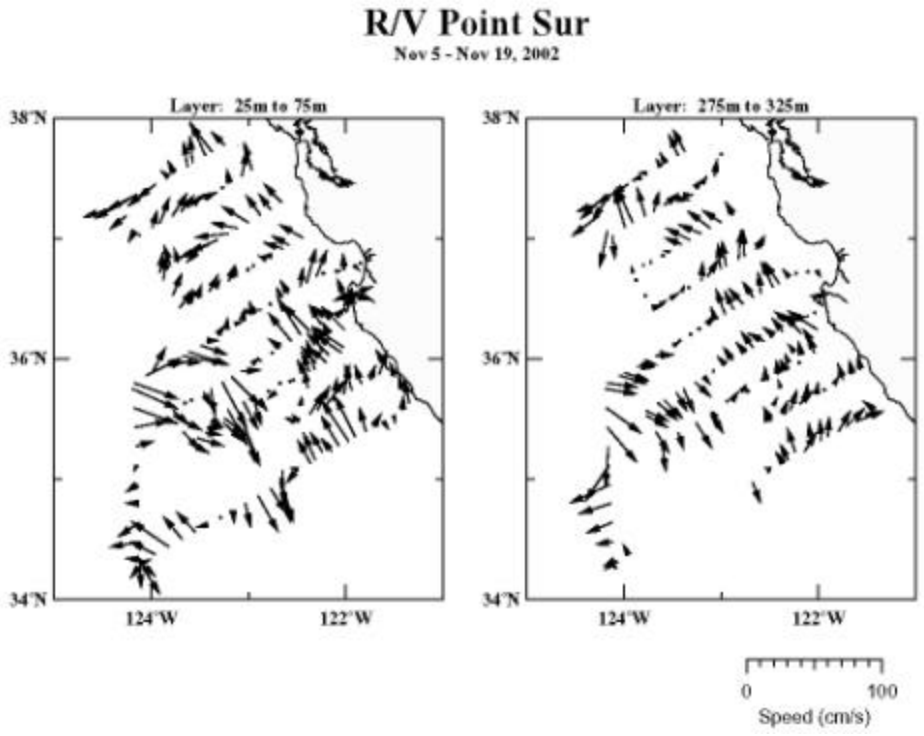

Figure III-13. VMADCP results for the NAVOCEANO cruise 5-19 November 2002. (left) The plot extends from 25 m to 75 m depth. (right) The plot extends from 275 m to 325 m depth. Arrows indicate magnitude and direction.

THIS PAGE INTENTIONALLY LEFT BLANK

IV. DISCUSSION AND SUMMARY

Off Central California, the transition of the coastal ocean from summer to winter is accompanied by a seasonal change in upper ocean water properties as cold saline waters are replaced by warm fresh waters of oceanic origin. This is accompanied by a deepening of the upper portion of the pycnocline next to the coast (a relaxation of summer upwelling conditions) and an increase in coastal sea level. The climatological record indicates that this transition is gradual in contrast to the transition that occurs in spring. Observations from the Hoke and NAVOCEANO cruises in the fall of 2002 elucidate the manner in which this transition occurs.

During summer, a dynamic trough separates the poleward undercurrent which flows along the continental slope from the equatorward flowing CC farther from shore. In fall of 2002, this trough was not uniform alongshore. At 1000 dbars, the trough appeared stronger off the Gulf of the Farallones than off Monterey and Point Sur (Fig III-11); at mid-depths, this asymmetry continued but was not as pronounced (Fig III-9). Between the two depressions, a ridge formed, which connected an offshore meander of the CC to coastal waters. Coastal flows subsequently advected these oceanic waters along the coast. The NAVOCEANO cruise observed these waters both to the north off the Gulf of the Farallones and to the south off Monterey Bay. The former appeared directly connected to the intrusion but the latter did not; however, the mooring off Monterey Bay indicated a reversal of the nearshore currents about the first of November. A dynamical connection between the CC meander and the formation of a ridge (flow) through the trough may exist but is beyond the scope of this thesis. A study of conditions in this region in spring (Baltz, 1997) noted a similar structure off the Gulf of the Farallones. In fall, 1990, Gezgin (1991) noted the appearance of fresh water near the surface at about the same location that it was observed in November 2002, i.e., to the southwest of the Gulf of the Farallones.

A. CC MEANDER

The California Current is described as a broad, shallow, equatorward current, extending for approximately 1000 km from shore (Hickey 1998). The characteristic

maximum current velocities are found at or near the surface (Lynn and Simpson 1987). As a surface current, its properties generally extend from the surface to approximately 300 m in depth. This was not the case in the surveys described in this thesis. Figure III-11 shows the properties of the 1000 dbar surface for the NAVOCEANO cruise. Salinity ranged from 34.44 to 34.47, with the minima next to the coast and offshore, associated with the meander/eddy (Fig III-11, upper right). The evident signature of the CC meander in these profiles showed that the properties of this meander extended to the bottom of the sampling box, i.e., at ~1000 dbar.

The isosteres, current vectors, and salinity distribution shape a clear picture of the circulation pattern during the fall of 2002. The observed CC flow was clockwise (anti-cyclonic) flow. Fresher waters from the CC meander divided the dynamic trough along 123°W. To the north and south of the ridge, two centers of fresher waters were observed. The northern center was connected to the CC meander by isosteres. It is speculated that the southern center was created in October by equatorward flow next to the coast. The flow next to the coast was predominately poleward, characteristic of the CCS.

Our data does not go far enough offshore to resolve the issue of whether or not the anticyclonic flow that we observed was a meander or eddy. RAFOS floats launched during the cruise may clarify this issue but they are not due to surface until 2006. Study of altimetric data may also clarify this issue. Our search of a local AVHRR data archive for the period of the cruises did not yield any suitable images. If the anticyclonic feature is an eddy, westward propagation would eventually bring it in contact with the CC again.

B. MINIMUM SALINITY

The upper and deep salinity minima were discussed in Chapter III. In Appendices B and C different techniques are used to describe their spatial variability. The upper minimum salinity seemed to trace the circulation patterns shown by both the VMADCP and the geopotential. Figure IV-1 shows the VMADCP vectors from the Hoke and NAVOCEANO cruises for 50 m to 100 m, overlaid on the minimum salinity. The region of particular interest is the meander, offshore between 35°N and 36°N and 123°W and 125°W. The vectors of greatest magnitude (~40 cm/s) are found at the center of low salinity (~32.6), as well as part of the outflow along the western edge of the eddy. The

direction of the currents around the low salinity feature showed a clockwise (anti-cyclonic) circulation pattern. Inshore of the eddy, the flow separated. On the eastern edge of the CC meander, there was a strong salinity gradient. The flow along this gradient was south to southeast. Inshore of the gradient there were alternating centers of low and high salinity (~33.2). The flow along these salinity centers was poleward (north to northeast).

On the northern edge of the eddy the flow was predominately onshore. Just onshore and north of the eddy the flow becomes eastward and northeastward, respectively. A region of high salinity surrounded the region of low salinity to the north. In the region of high salinity the flow was variable, with velocities to the west at the center and to the north on the southern edge. The flow in the center of low salinity feature off the Gulf of the Farallones was also variable from northeast to northwest. The separation in the flow occurred around Line 67 (~ 36^{o}N). Further inshore, the flow was predominately poleward along the coastline, with the vectors of greatest magnitude just outside the mouth of Monterey Bay (~ 30 cm/s).

Figure IV-2 shows the geopotential for 0-1000 dbar overlaid on the minimum salinity. Contours of geopotential for 0-1000 dbar are isosteres and represent streamlines for geostrophic flow at the surface assuming that the 1000 dbar surface is level. The highest values of the geopotential (~15.0 J/kg) occurred at approximately –124.3^{o}W and 35.6^{o}N, just south of the center of minimum salinity. The steepest gradient of geopotential was just inshore, to the north, over the center of lowest salinity (~32.6). Inshore and offshore of the eddy the contours of geopotential decreased in value, with the lowest values found at the southern end of the Hoke CTD line at ~12.8 J/kg and along the coast at 13.4 J/kg.

C. COLOCATION OF SUBARCTIC SURFACE AND INTERMEDIATE WATERS

The Subarctic character of the waters in the CC meander are reflected by salinity minima associated with both the surface waters and intermediate waters. To what extent are these features collocated? It is expected that the upper ocean salinity minimum would mix more quickly with the surrounding waters than with the deeper intermediate water. Appendices B and C and Chapter III use a variety of techniques to characterize the

Subarctic Surface and Intermediate waters. For the upper ocean salinity minimum, these include the minimum salinity, the pressure (depth) of the salinity minimum, the mean salinity of the upper 200 dbars, and the first principal component of salinity for the upper 200 dbars (see Appendix B). For the deep salinity minimum, the mean salinity of the 300-500 dbar layer was used as well as the first PC of salinity for the 300-500 dbar layer (Appendix B). Additional variables include the first PC for salt and spice for the entire water column. The correlation tables (Tables 3 and 4) below show how the features of the two salinity minimums correlate with one another.

Table 3. Upper salinity minimum

	Minimum Salinity	**P assoc. w/ Min Salinity**	**Mean Salt (0-200 dbars)**	**1st PC Salt (0-200 dbars)**	**1st PC Salt (0-1000 dbars)**	**1st PC Spice (0-1000 dbars)**
Min Salinity	1.000	-.7565	.8927	.8537	.8854	.6763
P associated with min salinity	-.7565	1.000	-.8384	-.8368	-.8443	-.7580
Mean salt (0-200dbars)	.8927	-.8384	1.000	.9546	.9954	.8645
1st PC Salt (0-200dbars)	.8537	-.8368	.9546	1.000	.9702	.8896
1st PC Salt (0-1000 dbars)	.8854	-.8334	.9954	.9702	1.000	.8739
1st PC Spice (0-1000 dbars)	.6763	-.7580	.8645	.8896	.8739	1.000

Table 4. Deep salinity minimum

	Minimum Salinity	**P assoc. w/ Min Salinity**	**Mean Salt (300-500 dbars)**	**1st PC Salt (300-500 dbars)**	**1st PC Salt (0-1000 dbars)**	**1st PC Spice (0-1000 dbars)**
Minimum Salinity	1.000	-.7565	.5594	-.1307	.8854	.6763
P assoc. w/ Min Salinity	-.7565	1.000	-.4555	-.0487	-.8443	-.7580
Mean Salt (300-500 dbars)	.5594	-.4555	1.000	-.1303	.5092	.4894
1st PC Salt (300-500 dbars)	-.1307	-.0487	-.1303	1.000	.0077	.1114
1st PC Salt (0-1000 dbars)	.8854	-.8443	.5092	.0077	1.000	.8739
1st PC Spice (0-1000 dbars)	.6763	-.7580	.4894	.1114	.8739	1.000

The properties of the upper salinity minimum were well correlated. With high values of correlation it was clear that the salinity minimum associated with the Subarctic surface waters dominated the water column. Conversely, the correlation values for the deep

salinity minimum were significantly lower (-0.0487, 0.0077). Low values indicate that the deep salinity minimum was not always present. The lack of correlation verified that the properties of the upper salinity minimum dominated the water column.

D. RECOMMENDATIONS FOR FUTURE WORK

This study illustrates the value of a data set which resolves mesoscale variability. It also demonstrates the need to sample as much of the water column as possible and the advantage of sampling as rapidly as possible. Further work on this data will benefit from the availability of altimeter and RAFOS data as well as use of the data with a numerical ocean model.

The role of the intermediate level circulation in the fall transition is poorly understood. At depth, the undercurrent slows in the fall and the resulting geostrophic adjustment results in the inshore portion of the lower pycnocline shoaling, (i.e. moving up while the seasonal pycnocline is deepening), resulting in an increase of the potential vorticity at intermediate pressures. This also results in a weakening of the dynamic ridge that lies adjacent to the slope. The slowing of the undercurrent reduces the rate at which equatorial waters are advected into the region. But hydrographic studies (Lynn and Simpson, 1987, Collins et al. 2003) show that most of the seasonal variability of subsurface water properties is caused by vertical movement of isopycnals and not by changes of water characteristics along isopycnals. How do these processes facilitate the onshore-offshore exchange that often occurs in late fall and winter?

Eastern boundary currents are complex regions. They are dominated by mesoscale variability and close to the coast, annual and interannual variability alters the character of the circulation system and the water masses. As a result they will require in situ data and models to predict the evolution of the environment in the foreseeable future.

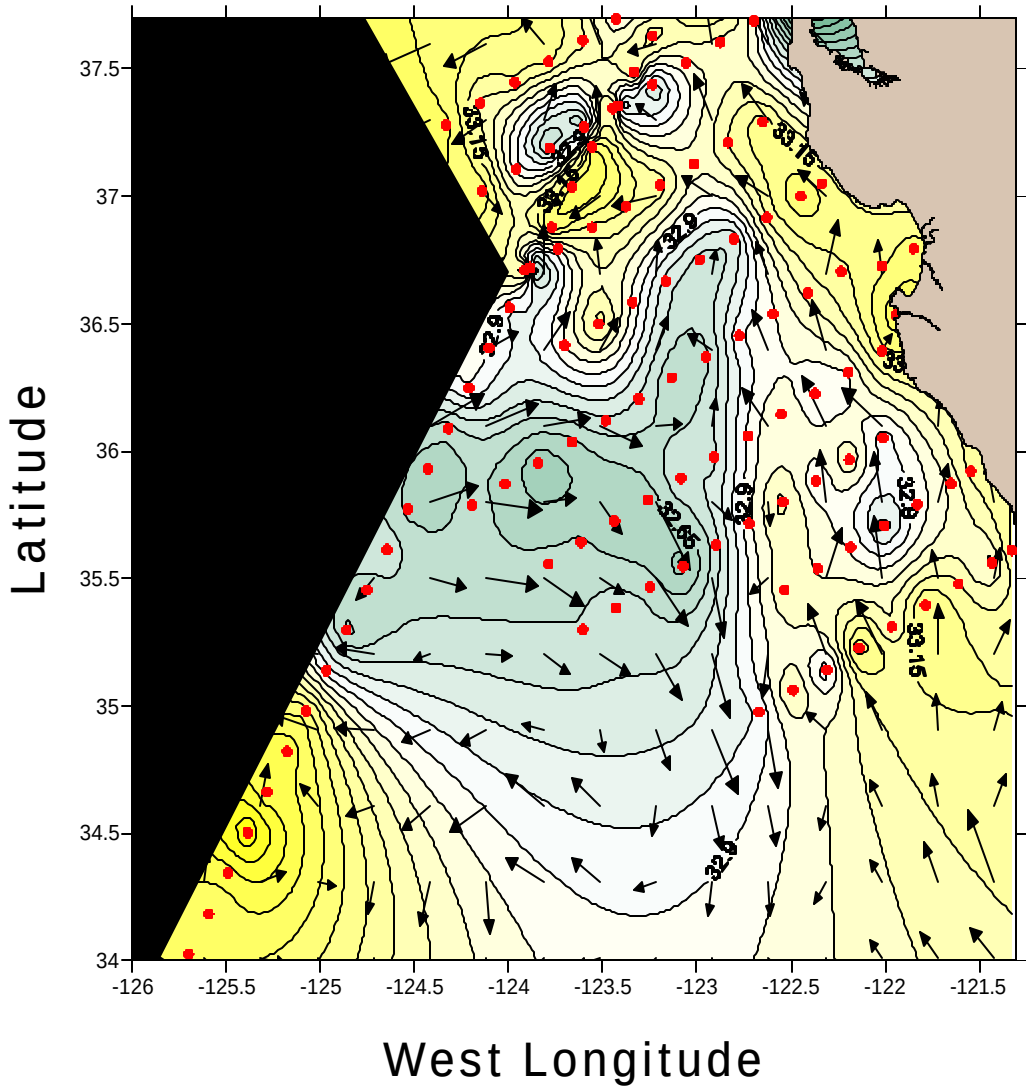

Figure IV-1. Minimum salinity in with u v current vectors overlaid for 50 m to 100 m. Contour interval is 0.05.

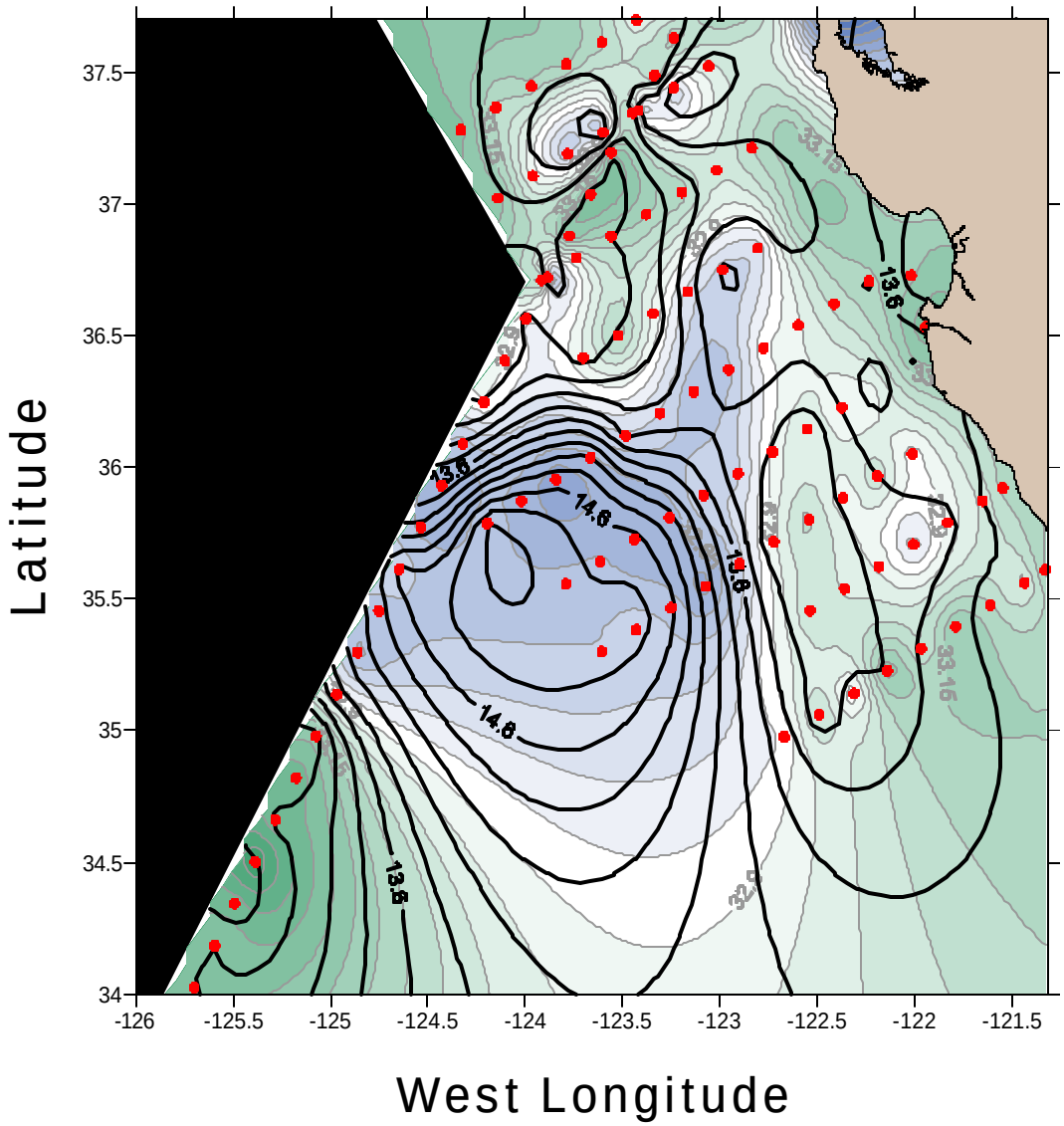

Figure IV-2. Minimum salinity in with 0/1000 dbar dynamic height thickness overlaid. Contour interval is 0.05 for the minimum salinity and 0.15 for the dynamic heights.

APPENDIX A. HIGH RESOLUTION SEA SURFACE TEMPERATURE AND SALINITY

The UDAS recorded average values of temperature and salinity every 50 seconds. The water for these samples came from a depth of about three meters. These data were used to produce high-resolution along cruise track charts shown in Figure A-1. For the NAVOCEANO cruise, results agree with those presented in Figure III-10. Because the cruise track extended to the southwest beyond the region of the CTD stations, the data showed the surface structure associated with the CC eddy where the ADCP data indicate a complex circulation pattern (Fig. III-13). The CC eddy showed clearly as a temperature maximum (~ 17^{o}C) along the outer portion of Line 67, the two hydrographic lines immediately to the south as well as along the southernmost hydrographic line (~16.5^{o}C) (Fig. A-1, upper left). Temperatures in the southeast corner indicated similar temperatures but did not clearly resolve the westward flow of the CC. For the Hoke cruise (Fig A-1, lower left), the region of the CC meander was indicated by a single sea surface temperature maximum (~17^{o}C) at about 35.7^{o}N. This was located between the onshore flow and the offshore flow at 50 m in the meander shown in Fig III-2.

Surface salinities for the NAVOCEANO hydrographic survey (Fig. A-1, upper right) agree well with those shown for the CTD data (Figure III-10, upper right). The offshore surface salinity minimum (S=32.7) associated with onshore flow in the CC meander was located in the core of the onshore flow at 36^{o}N (Figure A-1, lower right). This was exactly as seen in surface waters shown in Fig. III-1 where the outflowing meander waters were about 0.2 saltier than inflowing waters. The surface waters with S~32.7 were adjacent to and inshore of the temperature maximum along Line 67 and the two hydrographic lines immediately to the south. Despite strong winds, surface features associated with coastal upwelling and the CC meander were clearly shown in high resolution sea surface temperature and salinity data.

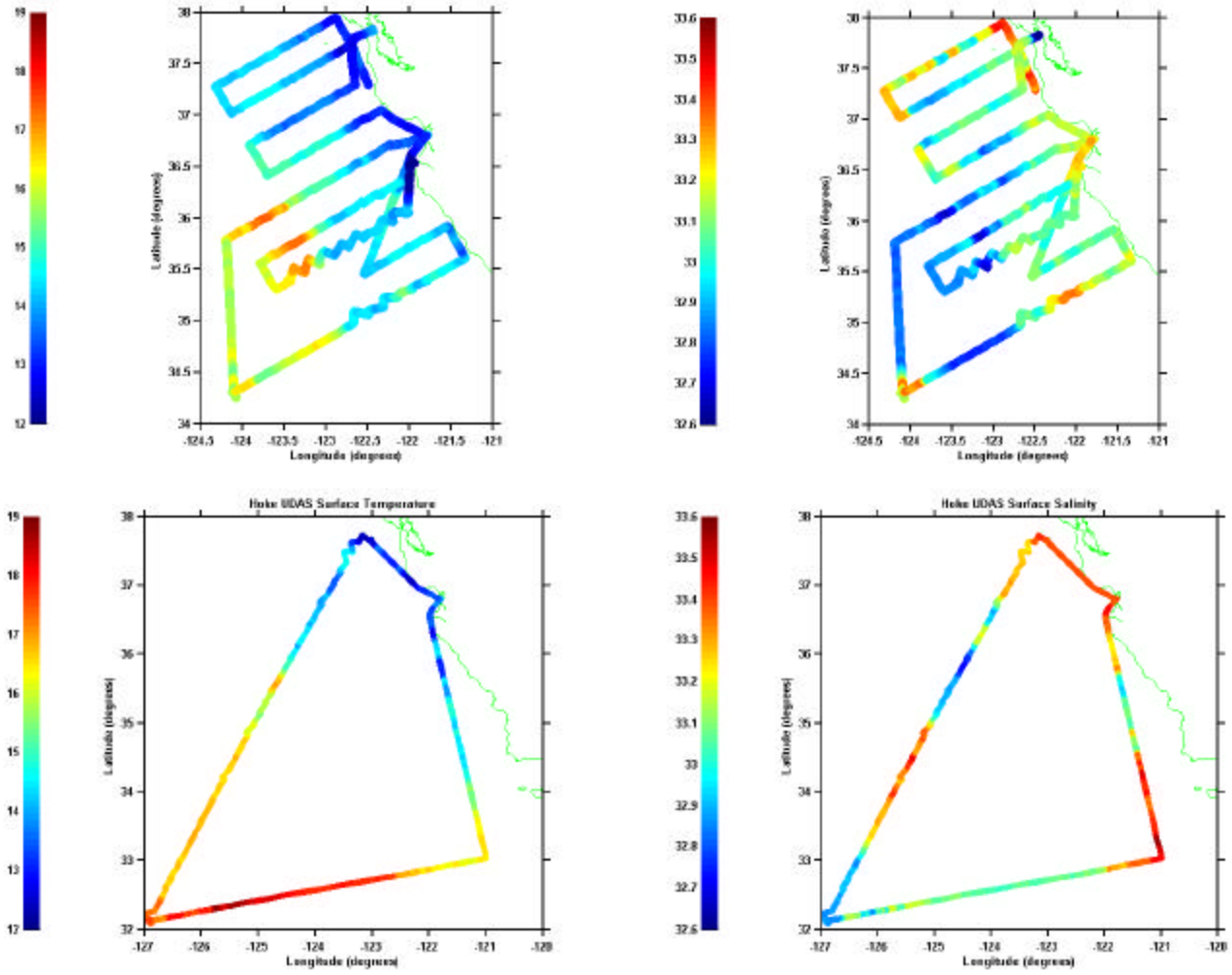

Figure A-1. UDAS plots of surface temperature and salinity along the ship's track. (upper left) The surface temperature (°C) recorded during the NAVOCEANO cruise. (upper right) The surface salinity, during the NAVOCEANO cruise. (lower left) The surface salinity recorded for the Hoke seamount cruise. (lower right) Surface temperature (°C) recorded for the Hoke Seamount cruise.

APPENDIX B. UPPER OCEAN SALINITY MINIMUM

Chapter III discussed the contrast between higher salinity waters upwelled at the coast and fresher Subarctic surface waters found offshore in the CC meander along the 25.0 kg m^{-3} isopycnal. Here three alternate methods of describing the upper ocean salinity minimum are tried. The first was the most direct: the minimum salinity and the corresponding pressure were extracted from each CTD cast. The second method was to average the salinity for the upper 200 dbar; stations shallower than 200 dbar were excluded. The final method also excluded shallow stations and used the first EOF for the upper 200 dbar salinity profile. The goal of the final two methods was to reduce the effects of small scale mixing processes on the property distributions.

The minimum salinity (Fig. B-1, upper left) showed fresher Subarctic waters intruding from the southwest toward the north along 123°W, approaching to within 50 km of the coast at 36.9°N. To the north and south of this intrusion, regions of minimum salinity were also observed offshore of the Gulf of the Farallones and to the south of Point Sur, either as separate eddies or possibly connected with the intrusion along 123°W. A strong salinity gradient existed at the boundaries of the intrusion of these surface Subarctic waters, with the strongest gradients located to the north. The maximum salinity observed was 33.3 next to the coast and north of San Francisco Bay. The minimum value of salinity was 32.6 (identical to that observed during the Hoke cruise) and was found at the center of the fresh water intrusion near 35.75°N, 123.5°W. The pressure of the minimum salinity (Fig B-1, upper right) showed higher pressures associated with fresher waters. Offshore, in the center of the fresh water intrusion associated with the meander of the CC, a maximum value of 95 dbars was observed. The minimum value was 4 dbars; minimum pressure values were located along the coast and to the northern and southern most ends of the survey. "Bulls eyes" surrounding individual stations existed in Fig B-1 (upper right), possibly indicating intrusive mixing (Lynn and Simpson 1990) or internal waves. The overall trend was for the salinity minimum to upwell toward the coast. As it shoaled into the mixed layer, the salinity increased by more vigorous stirring associated with air-sea interaction.

Because intrusive mixing processes may affect the location of the salinity minimum for individual stations, averages of upper ocean properties were used to try to trace the path of Subarctic surface waters into the coastal zone. The structure of the halocline and upper waters included profiles from the surface to 200 dbars (Fig III-5). The chart of the salinity averaged from 0-200 dbars is shown in Figure B-1, lower left. Features were similar to the chart of minimum salinity (Fig. B-1, upper left) although somewhat smoother as a result of the vertical averaging. The minimum value of 33.1 occurred offshore in the CC meander. The salinity minimum extended northward toward the coast, where it appeared to split at 36.5°N, with pools of salinity minimum to the north off the Gulf of the Farallones (S~33.35) and to the south of Point Sur (S~33.50). Maximum values (33.65) occurred to the north of San Francisco and appeared to flow cyclonically around the salinity minimum that was located to the west of the Gulf of the Farallones. A maximum value, 33.70, was observed at the southeastern corner of the survey.

The first principal component for the salinity of the upper 200 dbar accounted for 83% of the variance of the salinity. The amplitude of the first principal component is a measure of the deviation of an individual profile from the mean. The chart of the amplitude of the first principal component is shown in Fig B-1, lower right. The pattern of variability is similar to that for the salinity minimum (Fig. B-1, upper left) and the average salinity for the upper 200 dbar (Fig. B-1, lower left). As for those properties, the minimum, -0.24, occurred in the southwest corner of the chart and was coincident with the CC meander/eddy. The minimum extended northward along 123°W toward the coast where it seemed connected to the northwest with a minimum off the Gulf of the Farallones (-0.08) and to the southeast with a minimum south of Point Sur (0.0). The maximum values (0.12) occurred at 36.6°N, 123.5°W as well as at the southeast corner of the chart.

These three results yielded similar circulation patterns to those presented in Chapter III for the 25.0 kg m^{-3} isopycnal. It is not surprising that the advection and mixing of such a strong water mass feature was so robust.

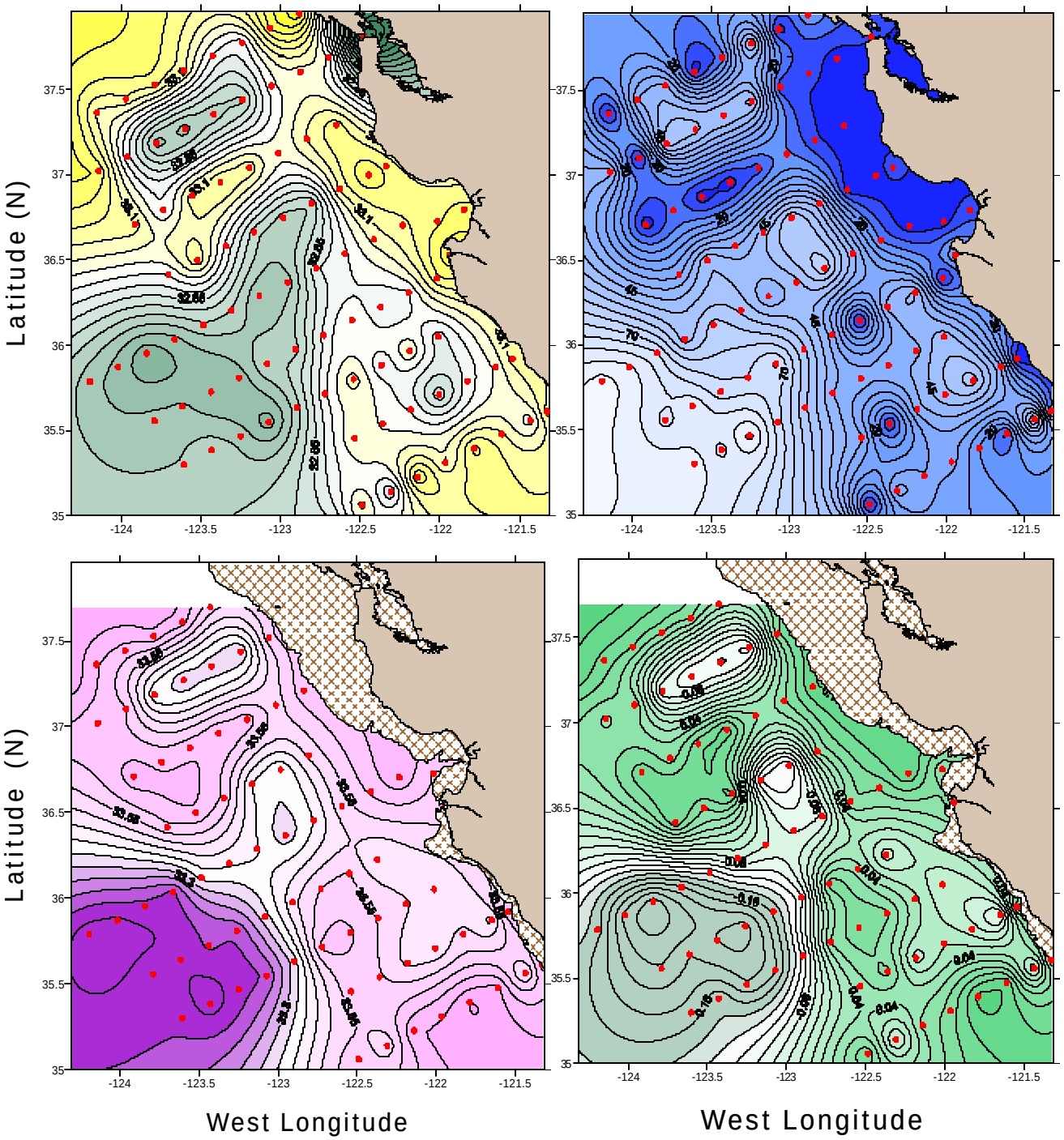

Figure B-1. Analysis of upper salinity minimum for the NAVOCEANO Cencal cruise with 200 m isobath overlaid. (upper left) Minimum salinity. Contour interval is 0.05. (upper right) Pressure of minimum salinity in decibars. Contour interval is 5 dbars. (lower left) Average salinity of the upper 200 dbars. Contour interval is 0.05. (lower right) Amplitude of the first principal component for upper layer (0-200 dbar). 83% variance is accounted for by the first PC Contour interval is 0.02.

THIS PAGE INTENTIONALLY LEFT BLANK

APPENDIX C. DEEP SALINITY MINIMUM

Figure C-1 uses statistical methods to describe the spatial distribution of the deep salinity minimum associated with Pacific intermediate water. The salinity minimum occurred within the 300 to 500 dbar layer and near the 26.8 kg m^{-3} isopycnal (Fig. III-8). The mean salt for the 300 to 500 dbar layer is shown in Fig. C-1 (left). The pattern of mean salinity variability closely resembled the pattern of salinity and spiciness on the 26.8 kg m^{-3} isopycnal. Maximum mean salinity (34.2) occurred along the inshore portion of the southernmost hydrographic line (Line 73) and extended north along 122.5°W and then to the east along the continental slope into Monterey Bay, surrounding a region of mean salinity minimum (<34.08) south of Point Sur. The mean salinity of waters along the CC meander was also low, <34.06. North of 36°N, the region of minimum mean salinity extended north along about 123.3°W, separating higher mean salinity waters along the slope to the east and offshore to the west.

The spatial distribution of the principal component for the first EOF mode is shown in Fig. C-1 (right). The first mode accounted for 56% of the variance. The pattern of its variability did not resemble the variability of other distributions. The maximum principal component amplitude (>0.1) extended parallel to the coast about 100 kilometers offshore but was interrupted by a minimum (-0.15) at 36.9°N, 123.5°W. The chart shows a number of data points appearing as a single minimum or maximum. Therefore, at this level, EOF analysis did not yield results consistent with either mean salt or salt or spice on a density surface.

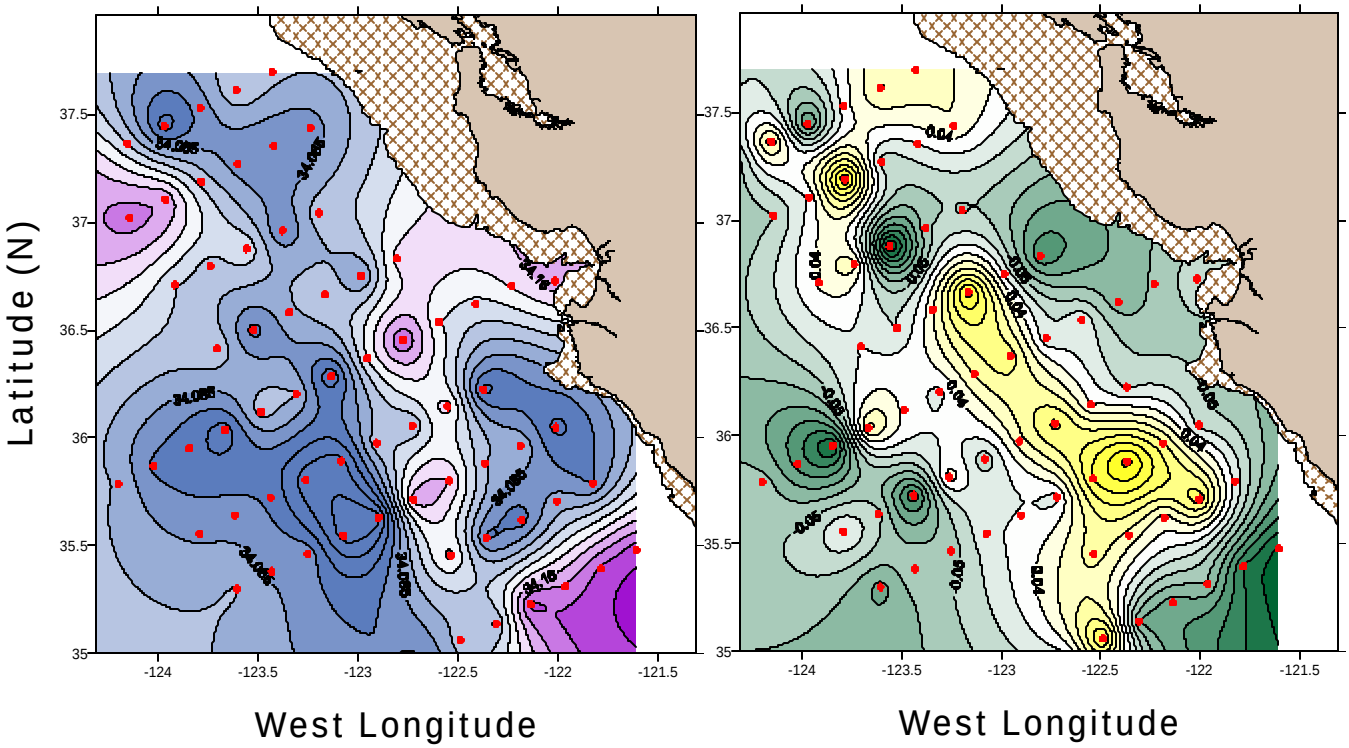

Figure C-1. Analysis of deep salinity minimum for the NAVOCEANO Cencal cruise. (left) Mean salt for 300-500 dbars. The contour interval is 0.015. (right) Amplitude of the first principal component of salinity for 300-500 dbars (56% of the variability). The contour interval is 0.03

APPENDIX D. DEEP SOUND CHANNEL

The deep sound channel (DSC) or SOFAR channel is a subsurface duct which makes possible the transmission of low frequency acoustic signals over a long range. The channel usually occurs where the speed of sound is the slowest, typically around 1480 m/s (Knauss 1997). The DSC exists because as depth increases temperature (and sound speed) decreases but below the thermocline, where temperature changes little with depth, pressure increases cause the sound speed to increase. A chart of the DSC for the Pacific Ocean between 40°S and 60°N shows the DSC axis around 500 dbars at 1488 m/s off the Central California Coast (Johnson and Norris, 1968). A more recent chart by J. L. Reid, Jr., indicated the DSC axis at about the same pressure off the central California coast but with a minimum speed of 1480 m/s (Munk and Forbes, 1989).

For the mean sound velocity profile (Figure D1, right), the DSC occurred at 586 dbar where the sound speed reached a minimum of 1480 m/s. In the pressure region around the minimum, the mean sound speed was nearly uniform. For example, from 500 dbars to 620 dbars the mean sound speed was 1480 m/s. In this region small changes of temperature could change the depth of the minimum but have lesser effect on the sound speed itself. The standard deviation of the sound speed was largest just below the surface, 6 m/s at 40 dbar. From 40 dbar to 156 dbar, the standard deviation decreased to 1.4 m/s but it then increased to a second maximum at 274 dbar, 1.8 m/s. Below this maximum, the standard deviation decreased to about 0.6 m/s. It remained at about this value between 800 and 1000 dbar.

The sound velocity profiles for all of the CTD stations from both cruises that extended to 1000 m depth are shown in Fig. D1 (left). A large amount of station-to-station variability occurred in the value of the sound speed for the DSC, however, the pressure of the minimum often fluctuated a large amount between adjacent stations. As noted above, the sound speed is relatively uniform near the minimum. Since the DSC lies at a depth where the contrast between NPIW and Equatorial waters is greatest, this is likely a result of intrusive mixing between these waters at the depth of the DSC. The spatial variability of the sound speed and pressure of the DSC are shown in Fig. D-2

(upper). The data from the Hoke cruise was included north of 35°N. The velocity of the sound channel (Fig. D-2, upper left) showed the lowest velocities offshore (~1477.7 m/s) in the dynamic trough described in Chapter III. The sound velocity increased toward the coast and offshore towards the CC eddy. Maximum velocities reached ~1480.7 m/s at the center of the CC eddy as well as near the mouth of Monterey Bay. The pattern of variability of the sound speed minimum resembled the distribution of density at 1000 dbars (Fig III-11, lower left) or the pressure (depth) of the 26.8 kg/m^3 isopycnal (Fig III-8, upper left). The latter indicates the importance of the shape of the pycnocline in determining the minimum sound speed of the DSC.

Although the sound speed minimum had a relatively smooth and consistent pattern, the chart of the DSC pressure (Fig. D-2, upper right) was noiser, and showed differences in the pressure of the DSC between adjacent stations of as much as 120 dbar. The linear relationship between the sound speed, c_{DSC}, in m/s and pressure, p_{DSC}, in dbars, was $c_{DSC} = 0.0048 p_{DSC} + 1476.6$ with a correlation coefficient of 0.46 so statistically, deeper sound channels had larger sound velocities. Low pressure (~ 480 dbars) dominated the region of the dynamic trough described in Chapter 3. Highest values of pressure were seen in the southeast corner along the inshore portion of the southern most hydrographic line.

In an attempt to overcome the noise in the DSC pressure, analysis of spatial variability of the DSC pressure require smoothing. Three approaches were considered: EOF analysis, polynomial curve fitting, and numerical filtering. The former approach was used because the code had been written for the salinity analyses described in Chapter 3. EOFs were computed for the sound velocity profiles between 400 and 800 dbar (Fig. D2, lower). The first and second principal components accounted for 83% and 8% of the variance respectively. The first principal component (Fig. D2, lower left) had a pattern similar to the pressure field (Fig. D2, upper right) but was just as noisy. The pattern for the second principal component (Fig. D2, lower right) was nearly uniform but bull's eyes appear at a number of stations. As a result, EOF analysis of sound speed profiles (Fig. D2, lower) did not appear to be superior to the description of the DSC properties (Fig. D2, upper).

Locally, properties of the DSC are controlled by the shape of the pycnocline. The minimum sound speed varied from 1477.8 to 1481.4 with larger speeds in the CC eddy and next to the coast and minima in the dynamic trough. The depth of the sound speed minimum was noisy, probably due to intrusive mixing between water masses, and ranged from 760 dbars to 430 dbars.

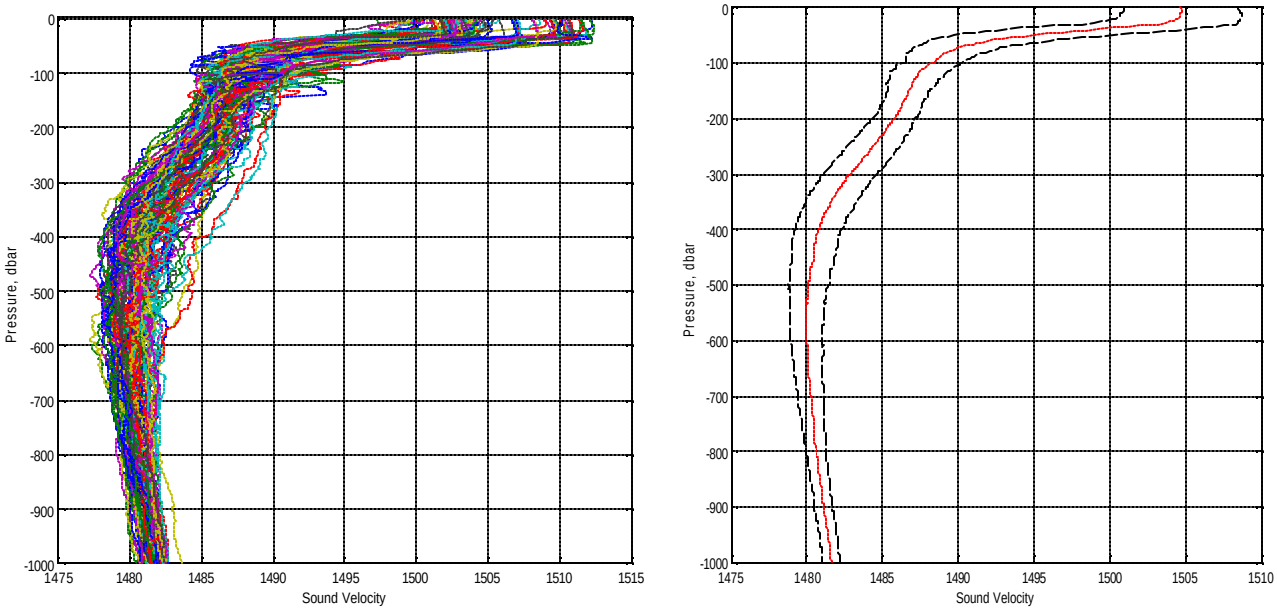

Figure D-1. Vertical Profiles. (left)Plot of the sound velocity against pressure in dbars. (right) Mean sound velocity (black line) ± one standard deviation. (red lines).

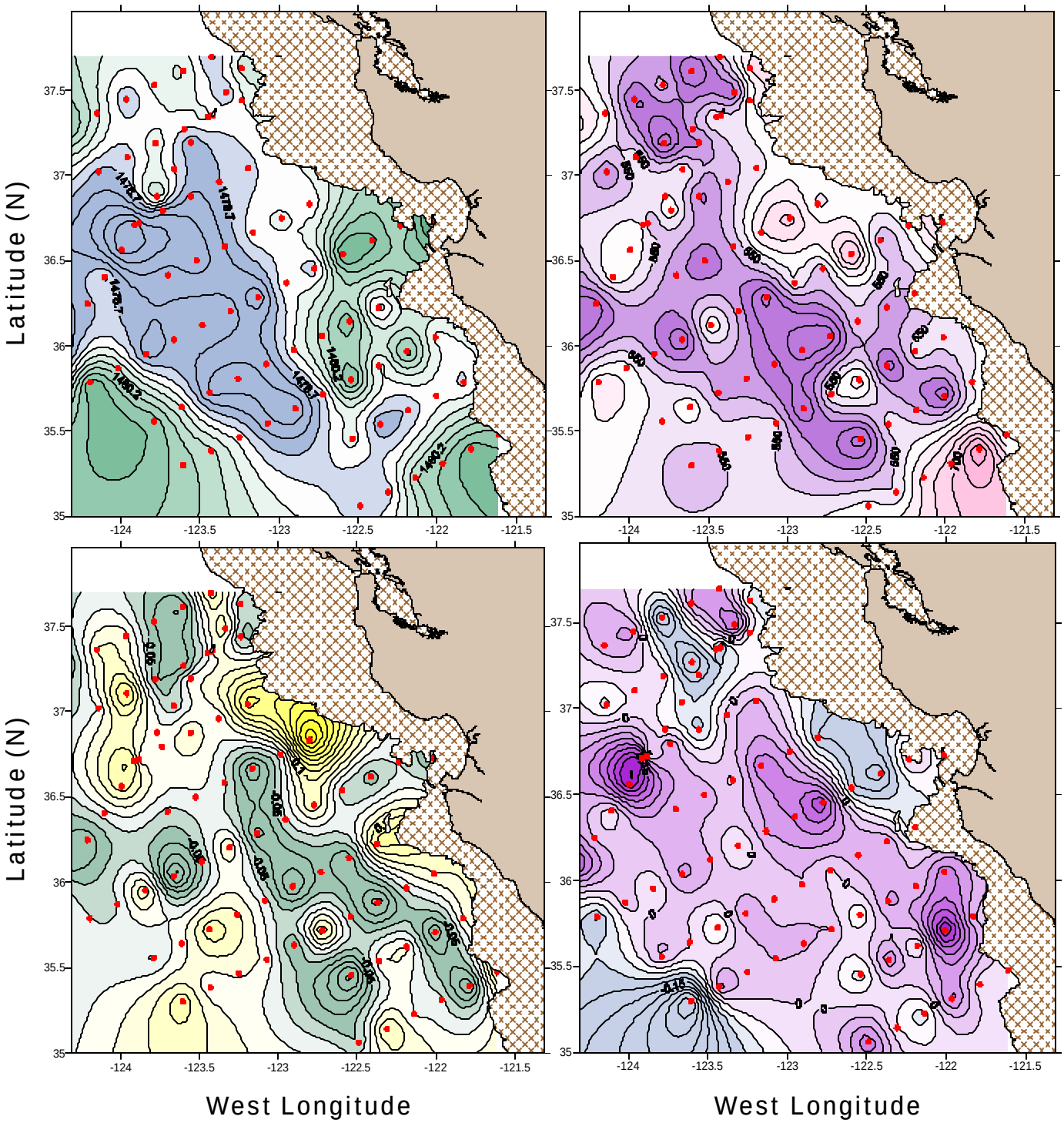

Figure D-2. Deep sound channel properties from 400 dbars to 800 dbars. The 1000 m isobath is overlaid. (upper left) Minimum velocity, contour interval is 0.3 (upper right) Minimum Pressure, contour interval is 30 dbars. (lower left) First PC, contour interval is 0.3. (lower right) Second PC, contour interval is 0.03.

THIS PAGE INTENTIONALLY LEFT BLANK

LIST OF REFERENCE

Baltz, K. A. *Ten Years of Hydrographic Variability off the Central California Coast During the Upwelling Season.* Master's Thesis. Naval Postgraduate School. Monterey, CA December 1997.

Chereskin, T.K. and M. Trunnell. 1996. *Correlation scales, objective mapping, and absolute geostrophic flow in the California Current.* Journal of Geophysical Research, Vol 101, No C10. 22619-22629.

Collins, C.A., C.G. Castro, H. Asanuma, T.A. Rago, S.K. Han, R. Durazo, and F.P. Chavez. 2003. *The California Current System off Monterey, California: Physical and Biological Coupling.* Deep Sea Research II, *in press.*

Collins, C.A., N. Garfield, T.A. Rago, F.W. Rischmiller, and E. Carter, 1997. *Mean structure of the inshore countercurrent and California undercurrent off Point Sur, California.* Deep Sea Research II 47. 765-782.

Dodimead, A.J., F. Favorite and T. Hirano.1963. *Oceanography of the Subarctic Pacific.* International North Pacific Fisheries Commisssion. Bulletin Number 13. 195pp.

Emery, W. J. and R. E. Thompson. *Data Anaylsis Methods in Physical Oceanography.* 319-40 pp., Pergamon, New York, 1997.

Fofonoff, N.P. 1985. *A New Salinity Scale and Equation of State for Seawater.* Journal of Geophysical Research, 90. 3332-3342

Flament, P. 2002. *A state variable for characterizing water masses and their diffusive stability: spiciness.* Progress in Oceanography. 54. 493-501.

Gezgin, E. 1991. *A study on hydrographic conditions and salt budget calculation for the Gulf of the Farallones with the data collected in August 1990.* Master's Thesis. Naval Postgraduate School. Monterey, CA. December 1991.

Hickey, B., M. 1998. *Coastal Oceanography of Western North America from the Tip of Baja California to Vancouver Island.* The Sea. Vol 11. 345-393.

Huyer, A., R.L. Smith, and J. Fleischbein. 2002. *The coastal ocean off Oregon and northern California during the 1997-8 El Nino.* Progress in Oceanography. 54. 311-341.

Jackson, J.E. 1991. *A user's guide to principle components.* New York: Wiley, 569 ppg.

Johnson, J. E. *An Assessment of Data Requirements for Quasi-geostrophic Nowcasts and Hindcasts of a Mesoscale Eddy Field in the California Current System with Application to Fall Transition.* Dissertation. Naval Postgraduate School. Monterey, CA June1990.

Johnson, R. H. and R. A. Norris. 1968. *Geographic Variation of Sofar Speed and Axis Depth in the Pacific Ocean.* Journal of Geophysical Research, Vol 73, No. 14. 4695-4700.

Joyce, T. M., 1989. *On in situ "calibration" of shipboard ADCPs*. Journal Atmos. Oceanic Technol., 6, 169-172.

JPOTS editorial panel. *Processing of Oceanographic Station Data*, 138 pp. UNESCO, Paris, 1991.

Knauss, J. A. *Introduction to Physical Oceanography*. Prentice-Hall, Inc., New Jersey, 1997.

Lamerdin, S. Personal communication. 2003

Lynn, Ronald J. and J. J. Simpson. 1987. *The California Current System: The Seasonal Variability of its Physical Characteristics.* Journal of Geophysical Research, Vol 92. No C12. 12947-12966.

Lynn, R. J., and J. J. Simpson. 1990. *The Flow of the Undercurrent Over the Continental Borderland off Southern California.* Journal of Geophysical Research, Vol 95. No C8. 12995-13008.

MBARI. Monterey Bay Aquarium Research Institute.
http://www.mbari.org/oasis/mooring_map4.jpg. December 2002.

Miller, A.J., J.C. McWilliams, N. Schneider, and J.S. Allen, J.A. Barth, and R.C. Beardsley. 1990. *Observing and Modeling the California Current System.* Transactions, American Geophysical Union, 80. 533-539.

Munk, W. and A. M. G. Forbes, 1989. *Global Ocean Warming: An Acoustic Measure*. Journal Physical Oceanography. 19:1765-1778.

Pickard, G.L. and W. J. Emery, *Descriptive Physical Oceanography,* 214 pp., Pergamon, New York, 1964.

Pollard, R. and J. Read, 1989. *A method for calibrating shipmounted Acoustic Doppler Profilers, and the limitations of gyro compasses*. Journal Atmos. Oceanic Technol., 6, 859-865.

Reid, J. L. and A.W. Mantyla. 1976. *The Effect of the Geostrophic Flow Upon Coastal Sea Elevations in the Northern North Pacific Ocean*. Journal of Geophysical Research. Vol 81, No. 18., 3100-3110.

Wust, G. and W.J. Emery. *The Stratosphere of the Atlantic Ocean*, 112 pp., Amerind Publishing, New Delhi, 1978.

INITIAL DISTRIBUTION LIST

1. Defense Technical Information Center
   Ft. Belvoir, VA

2. Dudley Knox Library
   Naval Postgraduate School
   Monterey, CA

3. Dr. Curtis A. Collins
   Department of Oceanography, OC/Co
   Naval Postgraduate School
   Monterey, CA

4. Mr. Thomas A. Rago
   Department of Oceanography, OC/Rg
   Naval Postgraduate School
   Monterey, CA

5. Dr. Mary L. Batteen
   Department of Oceanography, OC/Bv
   Naval Postgraduate School
   Monterey, CA

6. CDR Trish Moore
   Naval Postgraduate School
   Monterey, CA

7. CAPT J. Swakos, USN
   Department of Oceanography
   United States Naval Academy
   Annapolis, MD

8. Library
   Moss Landing Marine Laboratories
   California State Colleges
   Moss Landing, CA

9. Dr. J. Edward Johnson
   Technical Director
   Naval Oceanographic Office
   Stennis Space Center, MS

10. Library
Naval Oceanographic Office
Stennis Space Center, MS

11. Dr. Francisco Chavez
Monterey Bay Aquarium Research Institute
Moss Landing, CA

12. Dr. Steven Bograd
NMFS/PFEG
Pacific Grove, CA

13. CDR John Joseph
METOS.USW Program Officer
Naval Postgraduate School
Monterey, CA

14. ENS Colleen M. O'Malley, USNR
Delanson, NY

15. Dr. Robin Tomakian
Naval Postgraduate School
Monterey, CA

16. Dr. Leslie Rosenfeld
Naval Postgraduate School
Monterey, CA

17. Reginaldo Durazo
UABC Facultad de Ciencian Marinan
Ensenada, B.C., MEX

18. Mr. Rich Muller
Marine Operations
Moss Landing Marine Laboratories
Moss Landing, CA

19. Mr. and Mrs. Dennis O'Malley
Delanson, NY